PCCP

PERSPECTIVE

View Article Online
View Journal | View Issue

Cite this: *Phys. Chem. Chem. Phys.*, 2019, **21**, 13880

Photoinduced C–H bond fission in prototypical organic molecules and radicals

Michael N. R. Ashfold, *[a] Rebecca A. Ingle, †[a] Tolga N. V. Karsili [b] and Jingsong Zhang [c]

Received 5th December 2018,
Accepted 16th January 2019

DOI: 10.1039/c8cp07454b

rsc.li/pccp

Recent experimental and computational advances have heralded huge progress in the range and the detail of the database pertaining to photoinduced C–H bond fission processes. This Perspective provides a snapshot of the current state of knowledge as determined *via* gas phase (*i.e.* isolated molecule) studies of the primary photochemistry of families of hydrocarbon molecules (alkynes, alkenes, alkanes, aromatics and selected heteroatom containing analogues) and the corresponding radicals (including saturated and unsaturated hydrocarbon radicals). Different families show different and, in many cases, understandable propensities for dissociating from an excited electronic state or following non-adiabatic coupling (*i.e.* internal conversion) to high vibrational levels of the ground electronic state. The Perspective seeks to emphasise the potentially vast range of behaviours (dissociation timescales, product energy disposals, *etc.*) that can be expected to accompany internal conversion, reflecting the extent to which the tuning coordinate (*i.e.* the nuclear motions that tune the energy separation between the excited and ground state) projects onto the dissociation coordinate of interest (*i.e.* the breaking of the C–H bond).

1. Introduction

The recently concluded Cassini–Huygens mission has yielded a wealth of new data concerning the outer planets, their moons, and their atmospheres. The atmosphere of Saturn's moon Titan is now known to be composed mainly (~98%) of nitrogen, with methane making up most of the remainder. Molecules in the upper atmosphere of Titan undergo photodissociation, by absorbing short wavelength (vacuum ultraviolet, VUV) solar radiation, yielding radical species. These, in turn, undergo chemical processing, forming a plethora of heavier hydrocarbons like ethane, propane, ethene, acetylene, methylacetylene, *etc.*, and nitriles like hydrogen cyanide, acetonitrile, cyanoacetylene, *etc.*[1–4] A quantitative knowledge of the primary photochemistry of such carbonaceous species is essential for any detailed analyses and modelling of the atmospheres of the outer planets and of moons like Titan.[5]

Photoinduced C–H bond fissions are also of fundamental interest. The recent literature contains numerous articles, theoretical and experimental, that highlight the central role of excited states formed by electron promotion to an antibonding σ* orbital in facilitating bond fission.[6–9] Such states, formed by exciting an electron from an occupied lone pair (n) or bonding (π or σ) orbital, are now recognised as pivotal in discussions of the UV photofragmentation dynamics in many broad families of molecules. Exemplars include: water, alcohols, phenols, ethers and their thio-analogues; ammonia, amines, azoles, *etc.*; unsaturated molecules like hydrogen cyanide, acetylene and their derivatives; and alkyl and aryl halides.[7,10] nσ*/πσ* excited states have also been implicated in UV photoinduced ring-opening processes, the dynamics of which are also now attracting interest.[11] Photoinduced C–H bond fissions in alkanes, as well as in alkenes, benzene and larger aromatic systems, are underrepresented in most such discussions, however. The present work, in which we review and attempt to systematize prior studies of photoinduced C–H (and, on occasion, C–R, R = alkyl, aryl, *etc.*) bond fissions in both closed and open shell (*i.e.* radical) organic species, seeks to rectify this deficiency. Note, we have not attempted a comprehensive review of all hydrocarbon (and related) photochemistry. The foci of this article are the title photoinduced bond fissions in neutral precursors and under gas phase (collision-free) conditions, though we do note rival fragmentation channels when appropriate.

Fig. 1 shows potential energy curves (PECs) for the ground and a few of the lower lying excited electronic states of (a) H_2, (b) methane and (c) acetylene that help set the scene for what follows. The highest (indeed the only) occupied molecular orbital (HOMO) in the ground ($X^1\Sigma_g^+$) state of H_2 is the $1\sigma_g$ orbital. Promoting one electron from this orbital to the antibonding

[a] *School of Chemistry, University of Bristol, Bristol, BS8 1TS, UK. E-mail: mike.ashfold@bristol.ac.uk*
[b] *Department of Chemistry, University of Louisiana, Lafayette, LA 70504, USA*
[c] *Department of Chemistry, University of California at Riverside, Riverside, California 92521, USA*
† Current address: EPFL SB ISIC LSU, CH H1 575 (Bâtiment CH), Station 6, CH-1015 Lausanne, Switzerland.

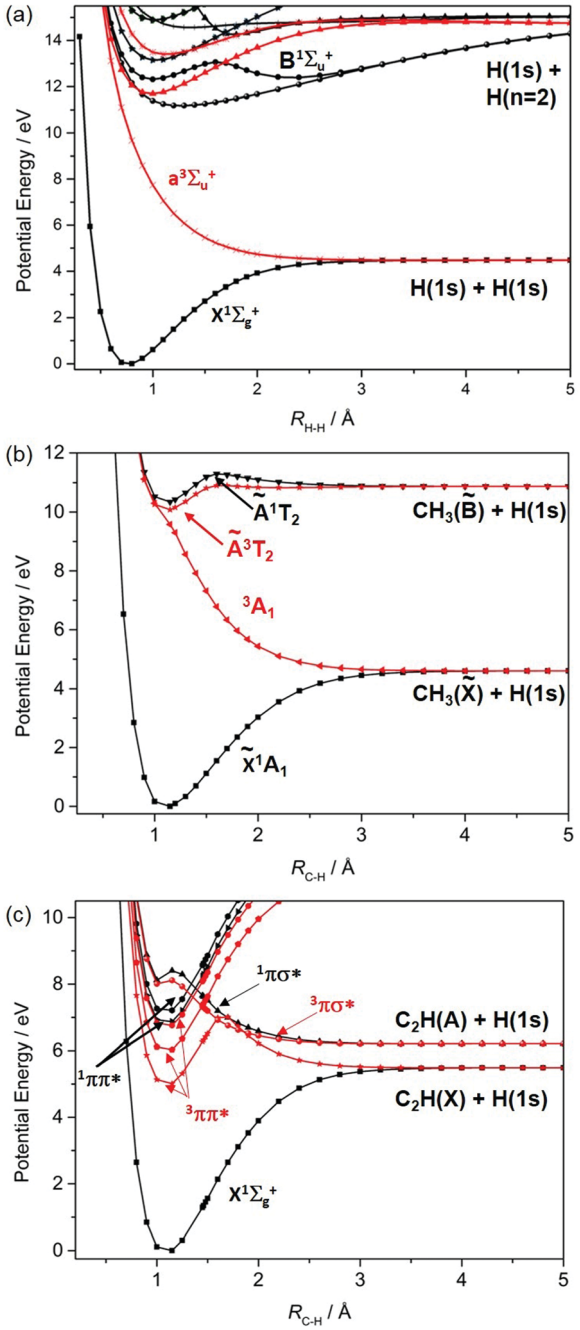

Fig. 1 Singlet (in black) and triplet (in red) PECs for (a) H_2 and, as a function of R_{C-H}, for (b) CH_4 and (c) HCCH. The latter two sets of curves are rigid body scans, calculated by progressively extending one C–H bond while holding the rest of the nuclear framework fixed at its ground state equilibrium geometry, with the constraint that the overall symmetry remains as C_{3v} and $C_{\infty v}$, respectively.

($1\sigma_u^*$) orbital yields the $a^3\Sigma_u^+$ excited state. As Fig. 1(a) shows, the PEC for this state is repulsive. The $a^3\Sigma_u^+$ state is dissociative and is one of just two states (the other being the ground state) that correlate with the asymptotic products H(1s) + H(1s). The lowest lying bound excited state of H_2 is the $B^1\Sigma_u^+$ state (attributable to a $2p\sigma_u \leftarrow 1\sigma_g$ orbital promotion), which correlates with the excited H(1s) + H(n = 2) products. [Note: all PECs reported here were calculated specifically for this article using the complete active space second order perturbation theory (CASPT2) method and MOLPRO2010.[12] To avoid breaking the narrative, details of the methods, basis sets and active spaces employed in the various calculations are collected in the Appendix.]

These PECs for H_2 were established long ago,[13] but are included to highlight synergies with a (limiting) cut through the multi-dimensional potential energy surfaces (PESs) for a saturated hydrocarbon like CH_4. Fig. 1(b) shows the relevant cut, calculated by stepping one C–H bond length (R_{C-H}), whilst holding the rest of the molecular framework at the ground state equilibrium geometry (*i.e.* retaining C_{3v} symmetry in this case). As in H_2, the lowest energy products (H(1s) + $CH_3(\tilde{X})$) each possess one unpaired electron but are otherwise non-degenerate. Their recombination yields one singlet state of CH_4 (the ground state) and a dissociative triplet state with an electronic configuration at large R_{C-H} that is dominated by a bond-localised $\sigma^* \leftarrow \sigma$ excitation. As we will see, such a $^3\sigma\sigma^*$ PES correlating to ground state products is a characteristic feature of all closed shell hydrocarbons. The first spin-allowed transition from the ground state of CH_4 is to a singlet state formed by promoting an electron from the t_{2g} HOMO to an orbital with substantial 3s Rydberg character in the Franck–Condon (FC) region. Fig. 1(b) shows this excited state correlating with an excited (Rydberg) state of CH_3 upon extending R_{C-H}. The much richer photofragmentation dynamics that prevail once the C_{3v} symmetry constraint is lifted are described in Section 2.4, while the photochemistry exhibited by $\tilde{B}$ state CH_3 radicals is detailed in Section 3.2.

Fig. 1(c) shows corresponding scans for the ground and first few excited states of C_2H_2, calculated by extending R_{C-H} with the remainder of the molecule maintaining its ground state (linear) minimum energy geometry. The additional state density (*cf.* CH_4) arising as a result of the π (HOMOs) and the antibonding π^* orbitals is obvious, as are the parallels with the corresponding PECs for the isoelectronic species HCN.[7] Unlike the CH_3 fragment formed upon C–H bond fission in CH_4, the C_2H radical formed by extending a C–H bond in C_2H_2 has two low-lying electronic states distinguished by whether the unpaired electron is in a pσ or pπ orbital. Fig. 1(c) shows that the former configuration constitutes the ground ($X^2\Sigma^+$) state of C_2H, and that the H + C_2H(X) products correlate with the ground state (and a dissociative $^3\sigma\sigma^*$ state) of C_2H_2. The low-lying $A^2\Pi$ excited state of the radical also forms both singlet and triplet states upon recombining with an H atom. These $^1\Pi$ and $^3\Pi$ states of C_2H_2 (in the linear limit) derive from $3s/\sigma^* \leftarrow \pi$(HOMO) excitations, *i.e.* excitations to states that have some 3s Rydberg character in the FC region but which acquire predominant σ^* antibonding character upon extending R_{C-H}. For compactness, we henceforth refer to such states simply as $\pi\sigma^*$ states. We also note that the first excited singlet (and triplet) states of C_2H_2 in the FC region arise from $\pi^* \leftarrow \pi$ excitations. These valence excited states are bound in the R_{C-H} coordinate, but have nonlinear minimum energy geometries and could predissociate by non-adiabatic coupling to one or more states that correlate with the lower energy asymptote(s).

We survey our current understanding of the UV photofragmentation dynamics of C_2H_2 and higher alkynes in Section 2.1, but a key distinction to note at this stage is the larger number of low-lying dissociation limits in a molecule like C_2H_2 (*cf.* the alkanes). Each dissociation limit in PE diagrams like those in Fig. 1 corresponds to a different electronic state of one or other dissociation product. In the specific cases featured here, one dissociation product is an H atom, the first excited state of which (with $n = 2$) lies 10.2 eV above the ground ($n = 1$) state. Thus, if we limit discussion to excitation energies below the ionisation limits of the molecules of interest (*e.g.* ~12.6 eV in the case of CH_4), the density of low lying product asymptotes is dictated by the electronic structure of the partner fragment. This is lower in a fragment like CH_3 (for which, apart from the one unpaired valence electron, there are only σ bonds) than in, for example, C_2H or HCO where the valence electrons also partition into less tightly bound π and, in the latter case, n orbitals. Indeed, much of the recent interest in molecular photofragmentations involving O–H (O–R), S–H (S–R) or N–H (N–R) bond fissions stems from conical intersections between PESs correlating to the various low-lying dissociation limits, and the non-adiabatic couplings enabled by these conical intersections.[7]

2. Hydrocarbon molecules

2.1 Acetylene, higher alkynes, alkyl analogues and nitriles

Acetylene (C_2H_2). $\pi^* \leftarrow \pi$ excitations are responsible for the long wavelength UV absorption of acetylene. C–H bond fission is observed following excitation of C_2H_2(X, $v = 0$) molecules at wavelengths $\lambda < 214.5$ nm[14] – corresponding to a photon energy ~600 cm^{-1} above the bond dissociation energy, D_0(H–CCH).[15] Energy conservation arguments dictate that the co-fragments formed when exciting at such long wavelengths must be ground (X) state C_2H radicals, and measurements of the parent excited state lifetimes,[16] their fragmentation probabilities,[17] the product energy disposal,[18] how these quantities vary with excitation wavelength,[19] and companion *ab initio* theory[20] all suggest that dissociation occurs *via* coupling to one or more of the nest of triplet states on a relatively long timescale (long when compared to a typical C–H vibrational period). C–H bond fission following excitation of vibrationally excited C_2H_2 molecules at longer wavelengths has also been reported (at $\lambda \sim 243.1$[21,22] and at 248.3 nm[23]).

Acetylene photodissociation has also been investigated by monitoring the H atom products formed at several shorter excitation wavelengths: at $\lambda = 193.3$ nm (still within the $\pi^* \leftarrow \pi$ band systems);[24] at $\lambda = 148.35$ and 151.82 nm;[25] at $\lambda = 121.6$ nm (the H Lyman-α wavelength)[26] and at several wavelengths in the range $121 \leq \lambda \leq 133$ nm[27,28] chosen to match with peaks in the parent absorption spectrum. All reveal formation of C_2H radicals in both their ground (X) and excited ($A^2\Pi$) states, with the latter dominating at the higher excitation energies. These C_2H(A) products are formed with extensive vibrational (predominantly in the C≡C stretch mode) but little rotational excitation, and the recoil velocities of the H atom partners are anisotropic (relative to the ε vector of the photolysis laser radiation). Emission attributable to C_2H(A) photofragments has also been reported following excitation at many wavelengths $\lambda \leq 125$ nm.[29] Such energy disposal is consistent with dissociation following excitation to, or efficient predissociation of the photoprepared Rydberg states by, the lowest dissociative $^1\pi\sigma^*$ state[7,25] depicted in Fig. 1(c). The H + C_2H(X) products formed at these shorter excitation wavelengths, in contrast, show isotropic recoil velocity distributions that peak at a low total kinetic energy release (TKER) and are generally consistent with that expected on the basis of (slower) unimolecular decay after radiationless transfer to high levels of the ground (X, or S_0) state.[28]

Diacetylene. Similar photofragmentation dynamics have been reported for diacetylene (HC≡CC≡CH). No radical products have been reported following long wavelength ($\lambda > 200$ nm) excitation of this molecule. Reactions involving metastable C_4H_2* molecules formed by such photoexcitation were touted as a possible route to forming the larger polyynes and polycyclic aromatic hydrocarbons that contribute to the haze that cloaks Titan,[30] but such a view was challenged following later measurements that showed that these C_4H_2* states have sub-μs lifetimes.[31] The TKER spectra of the H + C_4H products formed when exciting C_4H_2 at shorter wavelengths (in the range $127.5 \leq \lambda \leq 164.4$ nm) chosen to match with resolved Rydberg features in the parent absorption spectrum show peaks sitting on a continuous background.[32,33] Such structure reflects the formation of excited $C_4H(A^2\Pi)$ state radicals, with specific vibrational excitation in the CCC bend and C≡C stretch modes. As with C_2H_2, these products arise *via* non-radiative transfer to the corresponding $^1\pi\sigma^*$ continuum, while the underlying (isotropic) signal – that peaks at low TKER – is logically attributed to unimolecular decay of highly internally excited $C_4H_2(S_0)$ molecules.

Methylacetylene (and allene). The results of several early experimental studies of methylacetylene (propyne, $H_3CC{\equiv}CH$) photolysis at 193.3 nm were interpreted as showing acetylenic C–H bond fission as the dominant decay process,[34–36] as has also been suggested in one recent trajectory surface-hopping theoretical study.[37] However, H Rydberg atom photofragment translational spectroscopy (HRA-PTS) studies of propyne and its isomer allene (propadiene), at several wavelengths in the range $193.3 \leq \lambda \leq 213.3$ nm, returned essentially identical TKER spectra with a form that matched well with that obtained by assuming an approximate statistical model predicated on population of all possible vibrational states of the propargyl (H_2CCCH) product. Such behaviour was rationalised by assuming efficient coupling to high vibrational levels of the S_0 state and isomerisation (including H atom migration) prior to fragmentation.[38,39] This conclusion served to reinstate the original mechanistic proposal of Seki and Okabe,[40] and is consistent with (i) observations that both H and D atom products are formed, with essentially identical translational energy distributions, in the vibrationally mediated photodissociation of CD_3CCH using two photons with a total energy very similar to that of a single 193 nm photon,[41] and (ii) translational spectroscopy

studies of allene[42] and propyne[43] photolysis at 193 nm which both return a primary yield of H_2 products that was about one tenth that of the H atoms.

PTS studies of propyne and allene following excitation at shorter wavelengths (157 nm[44] and 121.6 nm[39]), in contrast, return isomer specific H atom velocity distributions. The photolysis of both molecules, at both wavelengths, yields H atoms with velocity distributions that peak at low KEs attributable to decay of highly internally excited S_0 molecules, but propyne also yields more H atoms with higher KE attributable to excited state acetylenic C–H bond fission – reminiscent of that seen in the short wavelength photolysis of both C_2H_2 and C_4H_2. Analysis of the photofragment fluorescence excitation spectra obtained following tuneable VUV excitation of propyne and allene also reveals isomer specific photodissociation dynamics at short excitation wavelengths.[45] Though outside the scope of a review focussed on photoinduced C–H bond fissions, we note that both CH_3 and CH_2 products have also been reported in the 157 nm photolysis of propyne, but the dynamics of the C–C bond fission process(es) leading to these products remains unclear.[44]

Cyanoacetylene. Cyanoacetylene (HCCCN) is isoelectronic with diacetylene, and the limited available data hints at similar photochemistry. In both cases, the long wavelength absorptions arise from $\pi^* \leftarrow \pi$ excitations, H atom loss is the lowest energy dissociation channel, and the energetic threshold for C–H bond fission lies above the onset of long wavelength absorption. Ion imaging studies return essentially identical H atom velocity distributions when cyanoacetylene is excited at 243.2 nm or at 121.6 nm.[46] This finding can be rationalised if the products observed at the longer excitation wavelength are the result of a two photon absorption process. Again, the derived TKER distributions are most readily explained in terms of unimolecular decay of highly internally excited S_0 molecules formed *via* non-adiabatic coupling from the state(s) populated at a total excitation energy of $\sim$10.2 eV.

H + C_3N fragments are the major dissociation products when cyanoacetylene is excited at 193.3 nm, but the low quantum yield estimated for this channel (0.3 ± 0.05) implies substantial population of metastable excited states.[47] The TKER distribution of the H atom products derived from ion imaging studies is intriguing.[46] The energy provided by a 193 nm photon is $\sim$0.6 eV above the calculated C–H bond dissociation energy, D_0(H–CCCN). Necessarily, therefore, the H atoms are slow, but their velocity distribution is sharply peaked and implies a substantial partitioning of the available energy (*i.e.* the photon energy less the bond dissociation energy) into product translation. Such energy disposal is characteristic of dissociation on a repulsive excited state PES, encouraging the suggestion that the photofragmentation of cyanoacetylene following excitation at 193.3 nm proceeds *via* coupling to the $^1\pi\sigma^*$ continuum. Analogy with C_2H_2, C_4H_2 (see above) and HCN (see below) has further encouraged the suggestion that the C_3N partner fragments are formed in the first excited $A^2\Pi$ state,[46] but the energy resolution of the data reported thus far is insufficient to allow substantiation of this prediction.

Hydrogen cyanide. Like the alkynes, the long wavelength absorption of HCN is attributable to $\pi^* \leftarrow \pi$ excitations. The threshold energy for forming H + CN($A^2\Pi$) products corresponds to a wavelength λ = 190 nm. C–H bond fission following excitation at λ = 193.3 nm necessarily yields ground ($X^2\Sigma^+$) state CN radicals,[48] but CN($A^2\Pi$) products dominate when HCN is photolysed at 157 nm[49] and at 121.6 nm.[50,51] CN(A) products have also been observed following 220 nm excitation of HCN(ν_3 = 4) molecules – *i.e.* following dissociation from excited levels with a total energy equivalent to that which would be achieved by exciting ground state HCN molecules at $\lambda \sim 172$ nm.[52] Further evidence for the dominance of H + CN(A) products is provided by the observation of laser action on the CN(A$\rightarrow$X) system following broadband ($\lambda > 155$ nm) flash photolysis of HCN.[53] All such observations support the view that, almost irrespective of the initial state prepared by VUV photoexcitation, if it is energetically possible, the photodissociation of HCN is driven by non-adiabatic coupling to, and subsequent H–CN bond fission on, the $^1\pi\sigma^*$ PES.[7]

2.2 Ethene, higher alkenes, polyenes and carbonyl containing analogues

Ethene. Ethene (C_2H_4) shows a broad absorption at long wavelengths, assigned to $\pi^* \leftarrow \pi$ excitations,[54] and an obvious step increase in absorbance at $\lambda < 175$ nm, attributed to the onset of the $3s \leftarrow \pi$ Rydberg transition.[55] PTS studies at 193 nm employing different H/D isotopomers of ethene identified both atomic and molecular hydrogen loss channels, with roughly equal probabilities, and some probability for loss of a second H atom from the primary C_2H_3 products.[56] The product translational energy disposals are consistent with unimolecular decay of internally excited S_0 molecules formed following internal conversion (IC) from the photo-prepared $^1\pi\pi^*$ state. Analogous studies at λ = 157 nm again identified both atomic and molecular hydrogen loss channels and deduced that most of the H(D) atoms formed at this wavelength arise from three body fragmentation processes. Again, the measured product branching fractions and energy disposals are in qualitative accord with expectations based on the unimolecular decay of C_2H_4 from high vibrational levels of its S_0 state,[57–60] though (weak) emission attributable to C_2H(A) radicals has been reported following excitation of C_2H_4 at photon energies above the threshold for three-body decay to H + H_2 + C_2H products ($\lambda < 144$ nm).[61]

Much recent effort has been devoted to unravelling details of the nuclear motions and couplings that drive IC from the $^1\pi\pi^*$ state to the S_0 state. Theory[62–65] has identified roles for two general classes of conical intersections, one in regions of configuration space associated with twisted and pyramidal geometries, the other near an ethylidene (CH_3CH) configuration that involves an H atom migrating across what (prior to photoexcitation) was the C=C double bond. The PECs shown in Fig. 2(a) have been calculated for a sequence of geometries along a linearly interpolated internal coordinate (LIIC) connecting the optimised ground state geometry to that of the minimum energy conical intersection (MECI) linking the $^1\pi\pi^*$ and ground state PESs, and are included primarily to illustrate the essentially barrierless

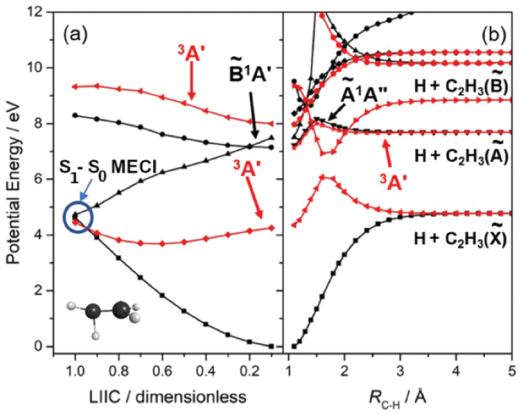

Fig. 2 Singlet (in black) and triplet (in red) PECs for C_2H_4. Panel (a) is for a sequence of geometries along a LIIC connecting the optimised ground state geometry to that of the MECI linking the $^1\pi\pi^*$ and S_0 PESs, the structure of which is shown. The curves shown in panel (b) are from a rigid body scan wherein R_{C-H} is extended at planar geometries, with the rest of the nuclear framework held at its ground state equilibrium geometry.

nature of this excited state decay route. Two molecular dynamics (MD) studies[64,66] also proposed a rival deactivation pathway *via* the $^1\pi$3s Rydberg state. Ultrafast pump–probe ion yield studies (involving both C_2H_4 and C_2D_4 excitation at 162 nm[67]) and a more recent ultrafast pump–probe photoelectron spectroscopy study (at 156 nm[68]) both serve to validate this suggestion, though another (at 159 nm[69]) found no evidence for the participation of any Rydberg state in the non-radiative decay of the $^1\pi\pi^*$ state. Excited state C–H bond fission involving nuclear motion on a $^1\pi\sigma^*$ PES analogous to that shown in Fig. 1(c), leading to electronically excited C_2H_3 radicals, should be possible at sufficiently high excitation energies – as shown in Fig. 2(b), and as noted long ago by Evleth and Sevin[70] – but we are not aware of any experimental demonstrations of such an excited state channel competing successfully with the ultrafast non-radiative decay to the S_0 state.

Higher alkenes. Replacing one or more of the H atoms in ethene by methyl groups leads to a progressive reduction in the ionisation potential and in the 3s←π excitation energy. Time resolved photoelectron spectroscopy studies following λ = 200 nm photoexcitation of *cis*- and *trans*-2-butene reveal ultrafast ($\tau \sim$ 20 fs) decay of the photoprepared $^1\pi$3s state by non-radiative coupling to the underlying $^1\pi\pi^*$ state and thence, on a longer timescale, to high vibrational levels of the S_0 state.[71] Similar studies of the fully methylated analogue, tetramethylethene, at several pump wavelengths around 225 nm, returned decay rates that are some 2- to 4-orders of magnitude slower.[71] Two dominant dissociation channels have been identified in the 193 nm photodissociation of isobutene (2-methylpropene), yielding H + C_4H_7 and CH_3 + CH_3CCH_2 products with relative yields and translational energy distributions that are broadly consistent with that expected for dissociation following non-radiative transfer to and intramolecular vibrational energy redistribution (IVR) on the S_0 state PES.[72]

PTS studies of propene (and selectively deuterated isotopomers of propene) following photoexcitation at λ = 157 nm identified no fewer than eight dissociation channels, of which the triple fragmentation to C_2H_2 + CH_3 + H products is dominant. The small kinetic energy releases and minimal recoil anisotropies of all products again imply that dissociation proceeds on the electronic ground state PES following non-radiative transfer from the photoexcited state.[73–75] Chin and Lee[76] reported relative probabilities (derived *via* RRKM calculations) for various two- and three-body decay channels of 1-butene molecules on the S_0 PES (calculated by electronic structure methods) at total energies appropriate for photoexcitation at 193 nm and 157 nm and predicted CH_2CHCH_2 + CH_3 radicals (*i.e.* products arising from a C–C bond fission after an initial H atom migration) as the dominant fragments at both excitation wavelengths.

Polyenes. Experiment (in the form of time-resolved, pump–probe studies of the initial excited state motions[77–81] and PTS studies of the eventual fragmentation products[82]) and theory (both electronic structure calculations[83,84] and MD simulations[85]) all imply ultrafast non-radiative decay following initial $\pi^* \leftarrow \pi$ photoexcitation of dienes like 1,3-butadiene and larger analogues like hexatriene and octatetraene, with eventual unimolecular decay from high vibrational levels of the S_0 state. Quantum-chemical plus RRKM calculations for 1,3-butadiene following excitation at both 193 nm and 157 nm predict more substantial roles for C–H bond fission channels than in the case of 2-butene (yielding both CH_3CCCH_2 and CH_2CHCCH_2 co-fragments) but, again, C–C bond fission (yielding CH_3 + CH_2CCH products after initial rearrangement to 1,2-butadiene) is identified as the dominant decay channel.[76]

UV excitation of cyclic dienes induces broadly similar photophysics. Theory (*ab initio* MD simulations)[86] and experiment (time-resolved photoelectron spectroscopy)[86,87] imply that the ultrafast non-radiative decay following $\pi^* \leftarrow \pi$ excitation in 1,3-cyclopentadiene, for example, is driven by initial (in-plane) motion along the bond-alternation coordinate followed by out-of-plane torsional motion about the C=C double bonds – similar to the nuclear motions that follow $\pi^* \leftarrow \pi$ excitation of C_2H_4[88] – to access a conical intersection with the S_0 PES. Photoinduced ring-opening of 1,3-cyclohexadiene following $\pi^* \leftarrow \pi$ excitation has been studied more extensively.[89–95] Again, the $^1\pi\pi^*$ excited state decays on an ultrafast timescale by non-adiabatic coupling (probably *via* an optically dark excited state) to the S_0 PES. Again, the topography of the PESs encourages C–C bond extension and torsion around the C=C double bonds, thereby priming the molecule to ring-open fully (to 1,3,5-hexatriene) or to revert to the ring-closed structure on the S_0 PES – albeit with sufficient internal excitation to fragment further. In both cases, the identity of final decomposition products remains an open question.

Nonetheless, the available data implies that the rates of non-radiative decay following $\pi^* \leftarrow \pi$ excitation of these C=C bond containing molecules (including allene[38,39,44] and fulvenallene[96,97]) are all so fast that rival excited state fragmentation pathways are unable to compete. Internal conversion to high vibrational levels of the S_0 state is the norm and C–H bond fission is a major decay pathway. But, increases in molecular size and in

excitation energy also translate into increased complexity: the number of energetically accessible product channels increases, as does the likelihood that some of these products are formed in multiple isomeric forms and may be susceptible to further (and possibly unintentional) photo-processing.

Aldehydes and ketenes. Formaldehyde (HCHO) and acetaldehyde (CH_3CHO) are isoelectronic with ethene and propene, respectively, but replacing a CH_2 group by an O atom has obvious photochemical consequences. Not least, the longest wavelength absorption in the aldehyde is an $\pi^* \leftarrow n$ transition originating from the O centred lone pair orbital, for which there is no equivalent in the corresponding alkene.

Formaldehyde. The minimum of the $S_1(^1n\pi^*)$ state of HCHO lies at an energy below the threshold for C–H bond fission (D_0(H–CHO) = 30327.6 ± 1.0 cm^{-1} (ref. 98)). H atoms are formed when exciting at energies above this threshold, but the parent absorption spectrum and the H atom photofragment excitation (PHOFEX) spectrum both show resolved rovibronic structure[99] consistent with the long (nanosecond) lifetimes of these S_1 levels. The detailed energy disposal in the H + HCO products formed following excitation in this near threshold region is parent level dependent, reflecting the relative probabilities of IC to highly excited S_0 levels and intersystem crossing (ISC) to the T_1 state. The T_1 PES shows a barrier in the R_{C-H} coordinate as the dominant configuration evolves from $^3n\pi^*$ to $^3\sigma\sigma^*$, the magnitude of which is overstated by the rigid body, planar constraints imposed when calculating the PECs shown in Fig. 3. Nonetheless, the presence of this energy barrier on the T_1 PES ensures that the IC pathway dominates at the lowest excitation energies, but the latter (yielding H + HCO products with a greater fraction of the available energy in the form of translational motion) gains in relative importance at energies approaching and above the top of the barrier.[100–102]

Most recent interest in HCHO photochemistry has focussed on the rival H_2 + CO molecular product channel and, particularly, unravelling signatures of the 'roaming' contribution to this product yield. Roaming in this case is now understood in terms of a frustrated C–H bond fission, wherein the H atom all but escapes from the long range attractive part of the S_0 PES, returns, re-encounters and reacts with the HCO partner to yield the molecular products.[103,104] The recent ion imaging studies[104] have also identified a three body fragmentation channel yielding H + H + CO products, with an energetic threshold of 35 410 cm^{-1}, which constitutes ~5% of the total product yield when exciting at λ = 266 nm. Dynamical studies of C–H bond fission following excitation of HCHO at shorter wavelengths are scarce, but *ab initio* theory – Fig. 3 in the context of motion along R_{C-H}, and prior coupled multi-surface photodynamics studies focussing on the C=O stretch and symmetric HCH bend coordinates[105] – indicate a wealth of non-adiabatic couplings and possible non-radiative decay pathways following excitation to the $^1\pi\pi^*$ and/or low-lying Rydberg states at wavelengths $\lambda < 180$ nm.

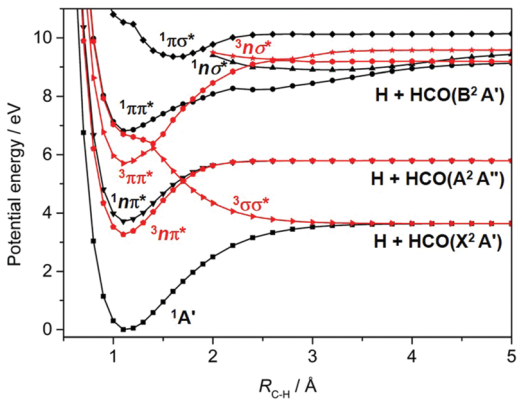

Fig. 3 Rigid body singlet (in black) and triplet (in red) PECs for HCHO plotted as a function of R_{C-H} for planar geometries, with the rest of the nuclear framework maintained at its ground state equilibrium geometry.

Acetaldehyde and other aldehydes. Ion imaging and IR emission studies of the CO products formed when exciting CH_3CHO at $\lambda > 300$ nm imply pathways to forming CH_4 + CO products involving both roaming H atoms and CH_3 radicals.[106,107] Contributions from three different C–C bond fission mechanisms have also been identified as the photolysis wavelength is reduced across the range $328 \geq \lambda \geq 265$ nm,[108] while recent experiments (cavity ring down absorption measurements of product quantum yields[109]) and theory (quasi-classical trajectory calculations[110]) both provide evidence for some C–H bond fission, associated with triple fragmentation to H + CH_3 + CO products, following excitation at λ = 248 nm. H atom photoproducts have also been reported following excitation at λ = 248 nm[111] and 205 nm.[112] PTS measurements following λ = 157.6 nm excitation of CH_3CHO identify C–C and aldehydic C–H bond fissions as the two dominant (out of a total of six) primary fragmentation pathways. Many of the primary HCO and CH_3CO products are formed with sufficient internal excitation that they undergo further unimolecular decay. Both the speed and the angular distributions of the various products imply that dissociation occurs after radiationless transfer to high levels of the parent S_0 state.[113] Analyses of the IR emission from CO fragments formed in the λ = 248 nm photolysis of propionaldehyde, isobutyraldehyde, and 2,2-dimethyl propanal have encouraged suggestions that the roaming route to forming molecular fragments becomes progressively more important with increasing parent molecular size.[114]

HCO radicals have been reported following long wavelength ($\lambda \sim 300$ nm) excitation of propenal (acrolein, CH_2=CHCHO) *via* its S_1–S_0 ($\pi^* \leftarrow n$) transition, and explained in terms of dissociation after intersystem crossing to the lowest triplet (T_1) PES.[115] PTS studies following excitation at shorter wavelengths (193 nm ($\pi^* \leftarrow \pi$ excitation)[116,117] and at 157 nm[118]) identify H + CH_2=CHCO and C_2H_3 + HCO as the dominant primary fragmentation pathways. Analysis of the product translational and angular distributions suggests roles for fragmentation following radiationless transfer to both the S_0 and T_1 PESs, but interpretation is complicated by the wealth of possible isomerisation and secondary fragmentation processes available at these high excitation energies.

H atom PHOFEX studies[119] and PTS studies following excitation of FCHO in the range $218 \leq \lambda \leq 248$ nm[120] and at

λ = 193 nm[121] all provide unequivocal evidence of aldehydic C–H bond fission. The operation of the rival F + HCO bond fission process was first deduced from analysis of the times-of-flight (TOFs) of H atoms formed by unintended UV laser photolysis of the partner HCO fragments[122] and then confirmed (at λ = 193 nm) by direct observation of the F atom and HCO radicals using universal ionization methods.[121] Theory[123,124] serves to confirm suggestions, based on the deduced product energy disposal, that the observed C–H bond fission occurs following ISC to the T_1 PES (the analogue of the T_1 ($^3\sigma\sigma^*$) PES shown for HCHO in Fig. 3).

In the case of alkenes, our summary identifies IC to high vibrational levels of the S_0 state and subsequent dissociation as the typical outcome following UV photoexcitation. Relative to the alkenes, the corresponding aldehydes have a lower lying $^1n\pi^*$ excited state. This state can be populated at energies close to the C–H dissociation limit, and typically shows orders of magnitude slower IC rates. This allows an opportunity for decay *via* (traditionally much slower) ISC to the T_1 PES, and the formation of ground state radical products with obviously non-statistical internal and/or translational energy distributions. The extent to which this photochemical difference persists when the simple aldehydes are excited at shorter (VUV) excitation wavelengths remains unclear.

Ketene. Ketene (H_2CCO) is isoelectronic with allene. The triplet and singlet $\pi^* \leftarrow \pi$ absorptions of ketene span much of the UV region, with the first (3s) Rydberg origin appearing at $\lambda \sim$ 215 nm. $^1CH_2$ (and $^3CH_2$) + CO are the dominant products formed following long wavelength (288 $\leq \lambda \leq$ 310 nm) excitation and subsequent IC to the S_0 (and ISC to the T_1) PESs.[125] Ion imaging studies of the CO products formed upon photolysis of H_2CCO at λ = 208 and 213 nm,[126] earlier studies of the IR emission from CO products formed by photolysis at λ = 193 nm,[127] and PTS studies of the H + HCCO products formed *via* photolysis in the range 193 $\leq \lambda \leq$ 215 nm,[128] all return product distributions that are broadly consistent with the decay of 'hot' S_0 parent molecules – in accord with later theoretical studies.[129,130] PTS studies at yet shorter wavelengths (λ = 157.6 nm), however, return a very different outcome. CH_2 + CO products represent ~97% of the total dissociation yield. The CO products show clear recoil anisotropy and energy conservation arguments suggest that the CH_2 partner fragments are formed in the excited $\tilde{b}^1B_1$ state.[131] Such observations would suggest that these products arise from C=C bond cleavage on a dissociative excited state PES.

2.3 Benzene and related aromatics

The UV photodissociation of many small aromatic hydrocarbons has been explored using a combination of multimass ion imaging techniques and complementary electronic structure theory.[132] Benzene (C_6H_6) is the exemplar. Long wavelength excitation populates the S_1 ($\tilde{A}^1B_{2u}$, $^1\pi\pi^*$) state *via* an electric dipole forbidden, but vibronically allowed, transition. The S_1 fluorescence quantum yield drops rapidly at wavelengths $\lambda <$ 244.5 nm, due to the opening of a new population loss process historically termed 'channel three'.[133] The mechanism

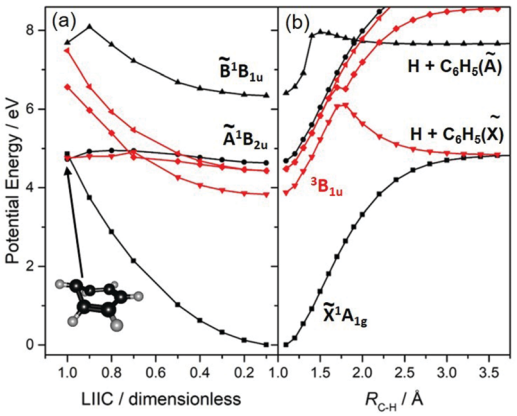

Fig. 4 Singlet (in black) and triplet (in red) PECs for C_6H_6. Panel (a) is for a sequence of geometries along a LIIC connecting the optimised ground state geometry to that of the prefulvenic MECI linking the $^1\pi\pi^*$ and S_0 PESs, the structure of which is included as an inset. The PECs shown in panel (b) are from a rigid body scan wherein R_{C-H} is extended at planar geometries with the rest of the nuclear framework fixed at its ground state equilibrium geometry.

of this decay has been a source of longstanding controversy, but recent ultrafast pump–probe photoelectron data have been interpreted as showing contributions from both IC to S_0 (*via* a conical intersection at prefulvenoid geometries) and ISC to low lying triplet states.[134] The PECs shown in Fig. 4(a), for a range of geometries along a LIIC connecting the optimised S_0 state geometry to that of the prefulvenic MECI between the S_1 and S_0 state PESs, support previous findings regarding the comparative 'flatness' of the S_1 PES (and a partner triplet PES) in this coordinate. Excitation at shorter wavelengths populates the S_2 ($\tilde{B}^1B_{1u}$, $^1\pi\pi^*$) state, and early PTS experiments identified C–H bond fission following IC to high vibrational levels of the S_0 state as the dominant (probably the exclusive) fragmentation process when exciting at λ = 193 nm.[135,136] H_2-elimination leading to formation of *o*-C_6H_4 is a less endoergic process, but the energy of the transition state *en route* to these products on the S_0 PES is too high for this rival decay channel to compete when exciting at λ = 193 nm. The prospects for excited state C–H bond fission in benzene appear somewhat like those for C_2H_4. As Fig. 4(b) shows, a rigid body scan in which one C–H bond, R_{C-H}, is extended while imposing planarity and holding the rest of the nuclear framework at the ground state equilibrium geometry shows the expected triplet ($^3\sigma\sigma^*$) repulsive PES correlating to the lowest dissociation limit, and identifies repulsive $^1\pi\sigma^*$ and (not shown) $^3\pi\sigma^*$ potentials correlating to the H + $C_6H_5(\tilde{A}^2A_1)$ limit.

Molecules like toluene[137] and *m*-xylene[138] show similar fragmentation behaviour following excitation to their respective S_2 states at λ = 193 nm, but experiments involving selectively deuterated precursors also reveal clear evidence for some isomerisation on the S_0 PES prior to eventual unimolecular decay by both C–C and C–H bond fission, yielding C_6H_5 + CH_3 and $C_6H_5CH_2$ + H products (in the case of toluene). Dissociation following IC to high levels of the S_0 state has been similarly advanced to account for the product energy disposals measured

following 193 nm excitation of, for example, ethyl-, *n*-propyl-, isopropyl- and butylbenzene.[132] Notably different dissociation dynamics have been reported following excitation to the S_1 states of ethyl- and *n*-propylbenzene at $\lambda = 248$ nm.[139,140] $C_6H_5CH_2 + CH_3$ and $C_6H_5CH_2 + C_2H_5$ products are still observed with appearance rates and kinetic energy distributions consistent with that expected for the dissociation of vibrationally 'hot' S_0 molecules. However, these are dwarfed by an additional yield of faster products that have been attributed to dissociation following ISC to the T_1 PES – reminiscent of the deduced involvement of both singlet and triplet decay pathways following UV excitation of benzene in the channel three region.

2.4 Alkanes

Methane. Detailed photochemical studies of alkanes are still relatively rare, in part because their absorption lies entirely in the VUV spectral region. H atoms from photolysis of CH_4 have been studied at $\lambda = 121.6$ nm[141–145] and at several wavelengths in the range $128 \leq \lambda \leq 133$ nm,[146] closer to the long wavelength onset of electronic absorption.[147] CH_3 and CH_2 product yields have been investigated by universal ionization mass spectrometry following CH_4 photolysis at 121.6 nm and 118.2 nm,[148] and electronically excited $CH_2(\tilde{b}^1B_1)$ products have been detected *via* their $\tilde{b} \rightarrow \tilde{a}$ fluorescence following excitation at $\lambda < 133$ nm.[149] H_2 products formed by two photon excitation in the range $210 \leq \lambda \leq 230$ nm have been investigated also.[142] Photoexcitation, at least at the lower energies within this range, promotes an electron from the $1t_2$ HOMO to the $3s/\sigma^*$ orbital. As Fig. 1(b) showed, the resulting S_1 state correlates with electronically excited CH_3 radicals upon extending R_{C-H},[150] but both *ab initio* electronic structure[151] and trajectory surface hopping dynamics[152] calculations confirm efficient non-adiabatic coupling to the S_0 PES.

Fig. 5 shows the geometries of two of the MECIs between the S_1 and S_0 PESs of CH_4 calculated using the global reaction route mapping (GRRM) method.[153–156] The lowest energy structures (of which CI1 is a representative) are sensibly consistent with dissociations evolving towards $CH_2(\tilde{a}^1A_1) + H_2$ products, the latter of which have been shown (experimentally) to be formed both rotationally and vibrationally excited.[142] The CI2 structure shown in Fig. 5 is reminiscent of that reported previously.[151] The experimental finding that the $CH_3(\tilde{X})$ fragments formed following excitation of CH_4 at, for example, $\lambda = 132.748$ nm (Fig. 6) carry high levels of *a*-axis rotational angular momentum[146] can be understood as the carry-over of the nuclear momenta developed *en route* from the FC region accessed by $S_1 \leftarrow S_0$ excitation to geometries like CI2. Experiment also reveals an increasing tendency for three-body fragmentation processes on tuning to shorter excitation wavelengths.[146,148]

As the upper panel of Fig. 6 shows, the $H + CH_3(\tilde{X})$ fragments display anisotropic, and TKER dependent, recoil velocity distributions.[143,146] Such an observation is not without precedent. Similar behaviour has, for example, also been reported for the $H + NH_2(\tilde{X})$ fragments from UV photodissociation of NH_3[157] and the $O + NO(X)$ fragments from photolysis of NO_2,[158] and is a natural consequence of angular momentum conservation when,

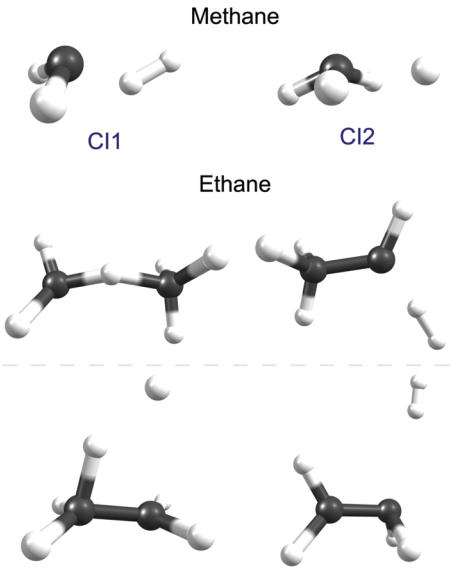

Fig. 5 Geometries of selected low lying conical intersections between the S_1 and S_0 PESs of CH_4 (upper) and C_2H_6 (below).

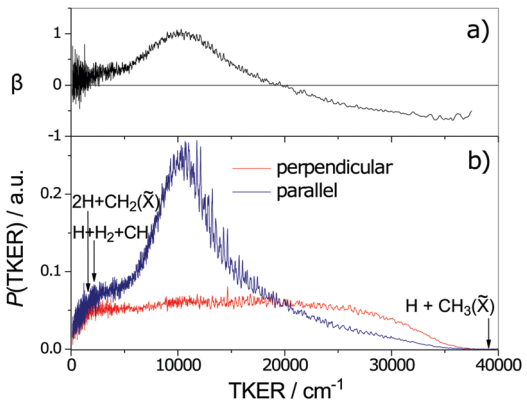

Fig. 6 TKER distributions derived from TOF measurements of H atoms formed in the 132.748 nm photodissociation of jet-cooled CH_4 molecules with the photolysis laser radiation polarised parallel (blue) and perpendicular (red) to the detection axis. The maximum possible TKERs of products arising *via* various three-body fragmentation processes are shown at the far left of the figure. Analysis of the fine structure evident in the TKER spectrum reveals that the $CH_3(\tilde{X})$ fragments are formed with high rotational angular momentum, preferentially about the *a*-inertial axis. (Adapted from ref. 146, with the author's permission.)

as here, the early time nuclear motions involve substantial motion transverse to the dissociation coordinate. Other striking aspects of the data shown in Fig. 6 include recognition that the decay of highly internally excited molecules formed by non-adiabatic coupling to the S_0 PES need not be 'slow', nor that the product branching ratios be anything like 'statistical', nor that the product recoil distributions be isotropic. In many of the cases considered in Sections 2.2 and 2.3, like ethene or benzene, the nuclear motions that facilitate IC to the S_0 state (*e.g.* torsion about the C=C bond, or ring puckering) are essentially orthogonal to the bond fission coordinates of interest. Thus the parent vibrational motions activated by coupling from the photoexcited

state to the S_0 state need to evolve (by IVR) before sufficient energy accumulates in any bond destined to break. This takes time, during which the molecule can sample much of the S_0 PES – as required for a 'statistical' fragmentation process. CH_4 illustrates the alternative behavioural extreme; non-adiabatic coupling *via* CI2, for example, involves passage through geometries that are on a clear path from the initial FC region on the S_1 PES to the H + $CH_3(\tilde{X})$ asymptote, and the fragmentation after IC can be as 'direct' and the product energy disposal as 'dynamically-determined' as any direct dissociation on a repulsive excited state PES.

Higher alkanes. Ethane is unique among the alkanes in that its electronic absorption spectrum, even at room temperature, shows resolved vibronic structure.[147] Electronic structure calculations have attributed the progression of features centred at $\lambda \sim 135$ nm to transitions originating from the near degenerate $3a_{1g}$ and $1e_g$ valence orbitals to orbitals with dominant 3p Rydberg character.[159] Such an assignment accords with quantum defect considerations, given the ionisation potential established by very recent pulsed field ionisation studies of jet cooled ethane.[160] The corresponding excitations to the 3s Rydberg state (including the analogue of the S_1–S_0 transition of CH_4) are predicted at lower excitation energies, and to be weak.[161]

An early photolysis study using the Xe resonance lines (λ = 147.0 and 129.5 nm) deduced the participation of (at least) three fragmentation pathways, two involving elimination of H_2 (with H_3CCH and H_2CCH_2 as the co-fragments) and another yielding CH_4 + CH_2 products.[161] As Fig. 5 shows, GRRM calculations identify suitable low-lying conical intersections between the S_1 and S_0 PESs of ethane to facilitate formation of each of these sets of products, plus another conical intersection consistent with direct C–H bond fission. H atom products have been reported following λ = 121.6 nm photolysis of both ethane and propane.[162] The H atom velocity distributions determined in both cases appear very similar – isotropic, peaking at low TKER and with a weak tail extending to higher kinetic energies. These observations have been rationalised by invoking initial C–H bond fission, yielding a fast H atom along with an electronically excited R* (*i.e.* C_2H_5* or C_3H_7*) fragment (analogous to the excited CH_3* product in Fig. 1(b)), followed by loss of a second (slow) H atom from the unimolecular decay of the primary R* fragment.[162] Validation of this suggested mechanism by high level theory is still awaited.

The electronic absorption spectra of propane and of the larger alkanes all stretch to longer wavelengths; unlike ethane, there is no symmetry reason why excitation from the HOMO to the 3s Rydberg orbital should be forbidden in these higher alkanes. PTS studies following 157 nm photolysis of propane have identified H, H_2 and CH_3 loss channels, each with significant branching fractions and each with different associated kinetic energy releases.[163] Experiments with selectively deuterated isotopomers revealed striking site specificities. Most of the H_2 photoproducts are eliminated from the central C atom, and recent trajectory surface hopping dynamics calculations suggest that the (much smaller) H_2 fractions attributed to 1,2- and 1,3-eliminations arise *via* 'roaming' mechanisms.[164] The PTS experiments also suggest that most of the H atoms originate from the terminal CH_3 groups, though Wu *et al.*[163] note that both three-body fragmentation channels and unintended secondary photolysis of the primary radical photofragments can complicate interpretation of the observed H atom signals. No CH_4 + C_2H_4 products were identified, despite this being the lowest energy product asymptote. Similarly detailed PTS studies of the H atom and H_2 products arising in the 157 nm photolysis of several larger straight-chain, branched-chain and cyclic alkanes have also been reported.[165] PTS studies of the 157 nm photolysis of cyclopropane identify C_2H_4 + CH_2 as the dominant dissociation products, but also measure a significant ($\sim$14%) yield of H atoms that are thought to arise *via* synchronous loss of two H atoms.[166] As with the *n*-alkanes, the H_2 yields from 157 nm photolysis of the branched chain and cyclic alkanes were found to gain in relative importance (*cf.* H atom loss) with increasing molecular size, hinting that the photodissociation dynamics of the larger alkanes is correlated with their flexibility and, in the cycloalkanes, with the ring strain. In all cases, neither the branching fractions nor the deduced translational energy disposals appear 'statistical' but, as the authors note, more theoretical investigations will be needed if we are to gain a detailed understanding of the fragmentation dynamics of these larger molecules.

Substituted alkanes. C–H bond fission has been reported following short wavelength photolysis of a number of substituted alkanes, including the alkyl halides CH_3I, CH_3Br and CH_3Cl at λ = 157 nm[167,168] and at λ = 121.6 nm,[169,170] and methanol at λ = 121.6 nm.[171] The TKER distributions returned by the HRA-PTS studies[170,171] show a fast component consistent with primary C–H (and O–H in the case of CH_3OH) bond fission and a (generally larger) slow component attributed to loss of two H atoms *via* a three-body fragmentation.

3. Hydrocarbon radicals

3.1 Methylidyne (CH) and methylene (CH_2)

The CH radical is included here mainly for completeness; ref. 172 lists many of the prior experimental and theoretical studies of this radical. As Fig. 7(a) shows, repulsive PECs attributable to $\sigma^* \leftarrow \sigma$ and/or $\sigma^* \leftarrow n$ excitations correlate to the H + $C(^3P)$ and H + $C(^1D)$ limits; wavelength dependent photodissociation cross-sections have been calculated for incorporation in astrophysical chemistry modelling.[173]

The photodissociation of CH_2 radicals has also been investigated theoretically.[174–178] The ground state of CH_2 has $^3\Sigma^-$ symmetry when linear, which reduces to $^3B_1$ at its bent equilibrium geometry. As Fig. 8 shows, in the linear limit, the ground state of CH_2 correlates with excited products (H + $CH(^4\Sigma^-)$) upon extending R_{C-H}, while the first excited triplet state (the $^3\Pi$ state formed by a $3s/\sigma^* \leftarrow n$ electron promotion) correlates with ground state (H + $CH(X^2\Pi)$) products. The degeneracy of the $^3A'$ and $^3A''$ components of the $^3\Pi$ state is lifted upon HCH angle bending. The $^3A'$ PEC is relatively insensitive to $\angle$HCH, but the

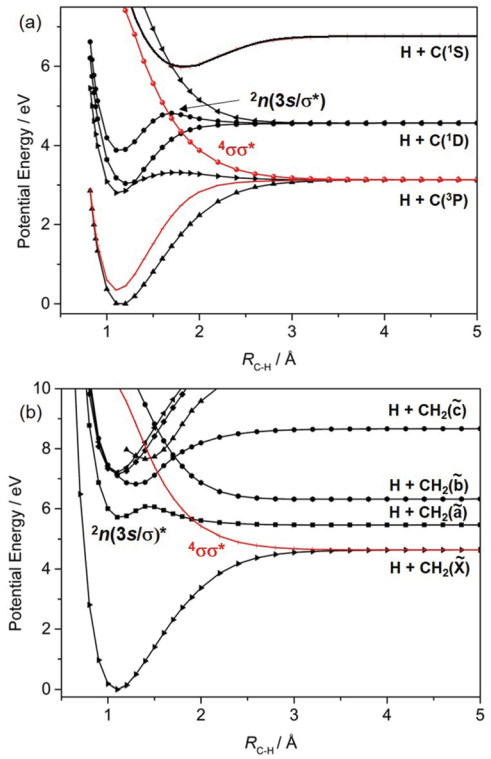

Fig. 7 Doublet (in black) and quartet (in red) PECs along R_{C-H} for the ground and first few excited states of (a) CH and (b) CH_3 radicals. The latter PECs were calculated by extending R_{C-H} at planar geometries, holding the rest of the framework at its ground state equilibrium geometry.

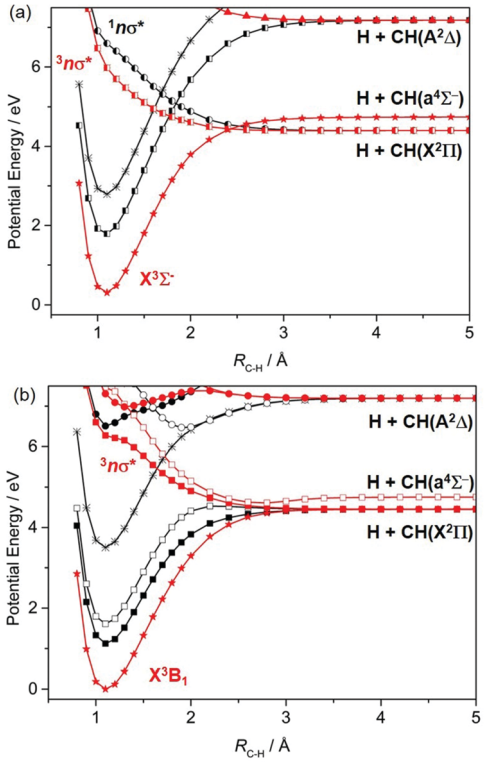

Fig. 8 Singlet (in black) and triplet (in red) PECs along R_{C-H} for the ground and first few excited states of the CH_2 radical for (a) $\angle$HCH = 180° and (b) $\angle$HCH = 133° (the equilibrium bond angle in the $\tilde{X}^3B_1$ ground state). States of ′ and ″ symmetry in (b) are distinguished by filled and open symbols, respectively.

crossing between the ground $^3\Sigma^-$ and $^3\Pi(A'')$ PECs develops into a conical intersection at extended R_{C-H}. The singlet PECs are more sensitive to changes in $\angle$HCH. Bending causes the first excited $^1\Delta$ state to split into its A′ ($\tilde{a}^1A_1$ at C_{2v}) and A″ ($\tilde{b}^1B_1$) components. Both interact strongly with the corresponding A′ and A″ components of the repulsive $^1\Pi$ ($3s/\sigma^* \leftarrow n$) state, with the result that both correlate adiabatically with ground state H + CH(X) products.

In terms of parent → product correlations, the lowest triplet and singlet states of the CH_2 radical show parallels with those for the analogous (singlet) states of H_2O or H_2S.[7] Long wavelength excitation to the $^3A'$ state of CH_2 can be expected to yield CH(X) radicals with modest internal excitation – as observed for the case of 193 nm photolysis of the CH_2(X) products arising in the near UV photolysis of H_2CCO.[179] Relative to H_2O or H_2S, $^3CH_2(\tilde{X})$ has an equilibrium bond angle much closer to 180°, so one can predict that molecules excited to the $^3\Pi(A'')$ state will also be likely to funnel through the conical intersection at linear geometries and dissociate to H + CH(X) products. CH_2 radicals photoexcited from the lowest singlet (ã) state will likely yield these products also, but analogy with H_2O or H_2S suggests that the resulting CH(X) fragments will be highly rotationally excited – given the large change in bond angle from the initial state ($\angle$HCH = 102°) required to reach the conical intersection at linear geometries and extended R_{C-H}.

3.2 Alkyl radicals

Methyl. In contrast to CH and CH_2, experimental studies have made substantial contributions to our knowledge of the UV photofragmentation of methyl (CH_3) radicals. The first excited state of CH_3 (which has $^2A_1'$ symmetry and is traditionally labelled as the $\tilde{B}$ state) is populated by promoting an electron from the singly occupied molecular orbital, the non-bonding carbon $2p_z$ orbital (n), to an orbital that is best viewed as 3s Rydberg in the FC region but gains increasing σ* anti-bonding valence character upon extending one C–H bond. The $CH_3(\tilde{B}–\tilde{X})$ absorption shows poorly resolved rovibronic structure, which is sharper in CD_3.[180] Photoexcitation within this band results in bond fission, yielding H(D) atoms together with $CH_2(CD_2)$ fragments. The atomic fragments show an anisotropic (perpendicular) recoil velocity distribution[181] – consistent with the $\tilde{B}–\tilde{X}$ parent transition assignment (*i.e.* the H(D) atoms recoil in the plane perpendicular to the parent transition moment, which is aligned along the C_3 axis) and the short excited state lifetime (~60 fs in the case of CH_3[182]). As Fig. 9(a) shows, excitation of the $CH_3(\tilde{B}–\tilde{X})$ origin transition (at λ = 216 nm) yields CH_2 fragments in their first excited $\tilde{a}^1A_1$ state (the lowest energy singlet state) with little rovibrational excitation.[181,183–185] Such an outcome matches theoretical expectations.[186,187] As Fig. 7(b) showed, the ground state of the CH_3 radical correlates with H + $CH_2(\tilde{X})$ products. The other parent state correlating to this lowest dissociation asymptote is a repulsive quartet state. The $\tilde{B}$ state of CH_3 correlates with H + $CH_2(\tilde{a}^1A_1)$ products (consistent with the experimental observation) and the very specific product energy disposal implies negligible non-adiabatic coupling

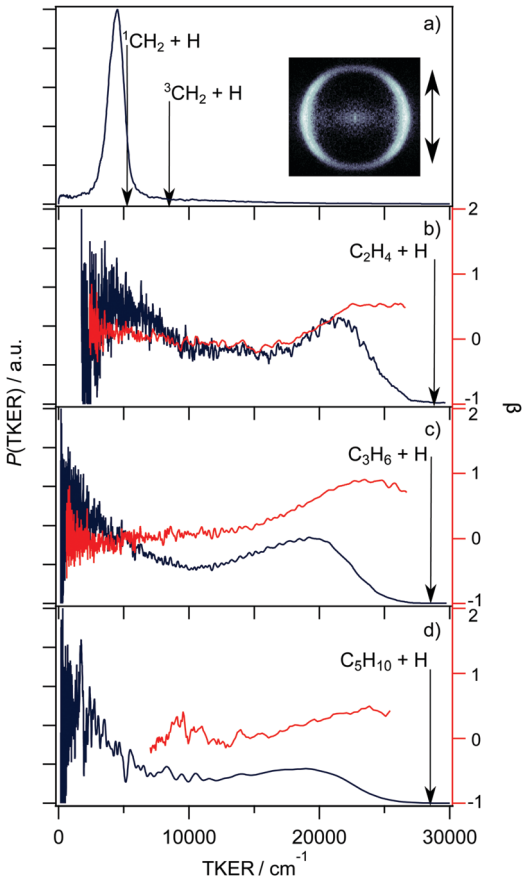

Fig. 9 TKER distributions (in black, left hand axis) and TKER dependent recoil anisotropy parameters (β, in red, right hand axis) derived from velocity or TOF measurements of H atoms formed by UV photoinduced C–H bond fission of the following alkyl radicals: (a) CH_3 at λ = 216 nm (with the H^+ ion image obtained with vertically polarised photolysis laser radiation shown alongside), (b) C_2H_5 at λ = 245 nm, (c) n-C_3H_7 at λ = 245 nm and (d) n-C_5H_{11} at λ = 240 nm. (Adapted from ref. 185, 188, 195 and 197, respectively.)

between the $\tilde{B}$ and $\tilde{X}$ state PESs in the regions of configuration space sampled during the dissociation process. But, tuning to somewhat higher excitation energies, the H atoms formed following (two photon) excitation to the $3p_z$ Rydberg state of the CH_3 radical are reported to show a broad, isotropic velocity distribution, peaking at low TKER values but extending to (and even beyond) the upper limit allowed by energy conservation, even when assuming ground state $CH_2(\tilde{X})$ as the co-fragment.[185] This very different energy disposal has been rationalised in terms of a sequence of non-adiabatic couplings that allow access to, and eventual dissociation on, the ground state PES.[185,187]

Larger alkyl radicals. The analogous $3s/\sigma^* \leftarrow n$ transition in the ethyl radical (C_2H_5) manifests as a broad, structureless absorption centred at ~245 nm. The H atoms from C_2H_5 photolysis within this band display a bimodal TKER distribution (Fig. 9(b)), with a fast component exhibiting (preferential) parallel recoil anisotropy, and a broad isotropic component peaking at low TKER.[188,189] Such observations are broadly in accord with previous theoretical predictions that C–H bond fission following excitation to the $\tilde{A}^2A'$ state in larger alkyl radicals (the analogue of the $\tilde{B}$ state of CH_3) could occur both directly – as in CH_3, but to relatively much more stable ($H + C_2H_4$) products in this case – and indirectly, following non-adiabatic coupling to the ground state *via* one or more of the conical intersections linking the parent $\tilde{A}$ and $\tilde{X}$ state PESs at distorted geometries.[186,190] Questions remain, however. Analogy with methyl (Fig. 7(b)) suggests that the PES associated with $3s/\sigma^* \leftarrow n$ electron promotion should correlate to $H + {}^1CH_3CH$ (*i.e.* methyl carbene (ethylidene)) products, the latter of which can isomerise to the minimum energy ground state structure (ethene), but theory[190,191] shows that the problem needs to be treated in higher dimensionality and that H atom ejection is preceded by H atom migration to a bridged excited state structure. Neither the H/D branching ratios measured when photolyzing partially deuterated ethyl radicals at λ = 250 nm nor the deduced production rate of the low TKER H/D atom products accord with expectations based on 'statistical' unimolecular decay from highly vibrationally excited ground state radicals.[189] Direct dynamics calculations have variously suggested roles for a minor channel leading to electronically excited triplet $C_2H_4(\tilde{a}^3B_{1u})$ + H products,[192] and for a roaming channel leading to $H_2 + C_2H_3$ products. These C_2H_3 products are then proposed to release an H atom, which could offer a possible rationale for the reported slow build-up rate of the atomic products,[193] though it is difficult to reconcile the observed H atom velocity distribution with such a mechanism.[194] Finally, we note that C–C bond fission is also thermodynamically allowed when exciting in this wavelength range, but we are not aware of any reports of such product formation.

The UV absorption spectra of the *n*- and iso-propyl radicals mimic that of the ethyl radical, as do the TKER spectra returned by HRA-PTS studies of these radicals at various wavelengths in the range $230 \leq \lambda \leq 260$ nm.[195] The TKER spectra are bimodal, as shown for the case of the *n*-propyl radical in Fig. 9(c), with fast (anisotropic, particularly in the case of *n*-propyl) and slow (isotropic) components. Again, the product TKER distributions stretch to much higher values than in the case of methyl radical photodissociation, reflecting the much greater relative stability of the H + alkene (*cf.* H + carbene) product pair.[195] Experiments involving partially deuterated propyl radicals show site-specific loss of the β H atom, confirming conclusions reached in earlier studies of the relative H and D atom yields following 248 nm photolysis of (selectively deuterated) *n*-propyl radicals formed by 222 nm photolysis of the corresponding bromopropane.[196] Again, the measured velocity distributions imply two dissociation pathways leading to the H + alkene (propene, in this case) products: one, wherein the photoexcited $n(3s/\sigma^*)$ state radicals evolve directly to ground state fragments, the other, indirect, involving unimolecular decay after non-adiabatic coupling to high vibrational levels of the ground state. The thermodynamic threshold for C–C bond fission in *n*-propyl (to $CH_3 + C_2H_4$ products) lies below that for C–H bond fission but there do not yet appear to be any studies reporting formation of such C–C bond fission products. Very similar PTS data has been reported for the $H + C_5H_{10}$ products from photolysis of the *n*-pentyl radical at wavelengths in the range $236 \leq \lambda \leq 254$ nm,[197] as illustrated in Fig. 9(d).

C–C bond fission is a significant contributor following UV photoexcitation of *t*-butyl radicals, however. The relative stabilisation of this radical by the pendant methyl groups is reflected in the lowering of its ionisation potential (6.87 eV,[198] *cf.* 9.84 eV for CH_3[199]) and of the energies of the associated excitations to Rydberg states. The UV absorption spectrum of the *t*-butyl radical shows well separated bands centred at $\lambda \sim 333$, 253 and 233 nm that have been assigned to, respectively, $3s/\sigma^* \leftarrow n$, $3p \leftarrow n$ and $3d \leftarrow n$ excitations.[200] Time resolved photoelectron spectroscopy data obtained following excitation at $\lambda = 330$ and 266 nm were interpreted as implying an important role for excited state C–C bond extension,[201] but PTS measurements were required to confirm the importance of both C–C and C–H bond fission pathways (yielding $CH_3 + CH_3CCH_3$ and $H + (CH_3)_2CCH_2$ products, respectively) following excitation at $\lambda = 248$ nm. Neither product TKER distribution nor the deduced product branching fraction approximate that expected on the basis of 'statistical' dissociation on the ground state PES[202] and later ion imaging studies[194] confirmed that the H atom photofragments from photolysis at wavelengths within all three of these UV absorption bands display bimodal velocity distributions reminiscent of those from photolysis of the smaller alkyl radicals. All of these data imply a substantial role for excited state C–H bond fission processes following UV photoexcitation of alkyl radicals.

Substituted alkyl (and related) radicals. The singly occupied molecular orbital in the ground state of the hydroxymethyl (CH_2OH) radical is traditionally viewed as a π_{CO}^* orbital[203,204] but, for simplicity, we persist with the n descriptor. The UV absorption spectrum of CH_2OH shows a broad feature spanning the range $380 \geq \lambda \geq 220$ nm, assigned to electron promotion from this orbital to a carbon centred 3s orbital, along with sharper structure attributable to $3p_x \leftarrow n$ and $3p_z \leftarrow n$ excitations (with respective origins at $\lambda \sim 285$ nm and ~ 244 nm). The breadth of the $3s \leftarrow n$ absorption is attributable to substantial $3s/\sigma_{O-H}^*$ valence mixing.[205] H atom photofragments are observed following excitation at all wavelengths within this range. Experiments with selectively deuterated hydroxymethyl radicals reveal O–H but no C–H bond fission (yielding formaldehyde as the molecular partner) at the longest excitation wavelengths. The H + HCHO products display a bimodal energy disposal. Most of the HCHO products are vibrationally (in the C=O stretch mode) and translationally excited, with an anisotropic recoil velocity distribution ($\beta \sim -0.7$), but a smaller fraction of the products shows much less translational and higher (undefined) internal excitation.[206]

All these products arise *via* non-adiabatic coupling at a conical intersection between the excited 2^2A ($^2n(3s/\sigma^*)$) and ground (1^2A) PESs at extended R_{O-H} bond lengths. Molecules that pass through this conical intersection upon increasing R_{O-H} are proposed to dissociate directly, yielding the translationally excited products. Conversely, dissociating molecules that initially follow the adiabatic path at the conical intersection have insufficient energy to access the $H + HCHO(\tilde{a}^3A_2)$ limit, resample the region of conical intersection, couple to the ground state and eventually dissociate to yield the more internally excited, less translationally excited products.[205] Fragmentations yielding both *trans*- and *cis*-HCOH products from photoinduced C–H bond fissions are identified with increasing (but still small) relative yields once above their respective formation threshold energies.[206,207] The measured energy disposals suggest that these HCOH products also arise from the decay of internally excited ground state CH_2OH radicals formed *via* non-adiabatic coupling at the $2^2A/1^2A$ conical intersection in the R_{O-H} stretch coordinate.

The fragmentation dynamics of the CH_2OH radical change markedly when exciting at energies in the region of the $3p_x$ and $3p_z$ Rydberg states. Now the excitation energies exceed the $H + HCHO(\tilde{a}^3A_2)$ dissociation limit, and an additional slow H atom yield is identified consistent with fragmentations that follow this adiabatic route past the $2^2A/1^2A$ conical intersection at extended R_{O-H}. The HCOH/HCHO product yield ratio increases when exciting on $3p \leftarrow n$ resonances, the (higher energy) *cis*-isomer is the favoured HCOH product, and the deduced energy disposal in the HCOH products is isomer-dependent and clearly non-statistical.[207] These findings have been rationalised by assuming initial excitation to both the 3^2A (3p) and 2^2A (3s) Rydberg states, the former of which can decay by passage through successive conical intersections in the R_{C-H} stretch coordinate *en route* to both *cis*- and *trans*-HCOH products in their respective ground states.[208]

The corresponding $3s \leftarrow n$ absorption of the 1-hydroxyethyl (CH_3CHOH) radical extends to $\lambda > 500$ nm. As with the CH_2OH radical, studies involving selectively deuterated precursors and long excitation wavelengths identify O–H bond fission (leading to fast H atoms with an anisotropic recoil velocity distribution along with CH_3CHO co-products) as the exclusive fragmentation channel, and theory[209] has again identified a conical intersection between the 2^2A ($^2n(3s/\sigma^*)$) and 1^2A (ground state) PESs in the R_{O-H} stretch coordinate that successfully explains this observation. A second, slow component apparent in the H atom velocity distributions measured following excitation at $\lambda \leq 320$ nm has been attributed to the onset of rival C–H bond fission yielding vinyl alcohol (enol) partner fragments.[210]

The methoxy (CH_3O) radical is an isomer of hydroxymethyl. C–O bond fission is the dominant outcome following photoexcitation of CH_3O radicals in the wavelength range $282 \geq \lambda \geq 267$ nm[211] and we have not found any reports of C–H bond fission following UV photoexcitation of CH_3O. The photodissociation of ethoxy (C_2H_5O) radicals and their deuterated analogues has been investigated, however, by PTS methods at three wavelengths in the range $208 \leq \lambda \leq 240$ nm, revealing the operation of three dissociation channels – yielding $H + CH_3CHO$, $CH_3 + HCHO$ and $OH + C_2H_4$ products – with roughly equal probabilities.[212] The product branching ratios, their respective TKER distributions, and the anisotropic recoil velocity distribution of, particularly, the $OH + C_2H_4$ products all suggest a non-statistical fragmentation process and that the necessary isomerisation to CH_2CH_2OH prior to OH loss probably occurs on an excited state PES.[212] Photodetachment of the ethoxide anion at $\lambda = 388$ nm yields ethoxy radicals, in both the $\tilde{X}^2A''$ and first excited $\tilde{A}^2A'$ states. A fraction of these radicals are formed

with sufficient internal energy to fragment, yielding CH_3 + HCHO products only. C–H bond fission would be possible on energetic grounds, but is not observed.[213]

Turning to the sulfur analogues, C–S bond fission has been observed following excitation of the thiomethoxy (CH_3S) radical in the wavelength range $360 \geq \lambda \geq 340$ nm and at $\lambda = 219$ nm.[214] C–H bond fission has also been recognised following excitation of CH_3S radicals in the ranges $213 \leq \lambda \leq 220$ nm[215] and $344 \leq \lambda \leq 362$ nm.[216] The co-fragment in both cases is H_2CS, and dissociation in the latter case is assumed to occur after IC to the ground electronic state (which, in this scenario, must occur in competition with the excited state predissociation to CH_3 + S fragments).[214]

3.3 Unsaturated aliphatic radicals (and related species)

Ethynyl. The ground ($^2\Sigma^+$) and low lying first excited ($^2\Pi$) states of the C_2H radical both have linear equilibrium geometries, while the next excited doublet state (the B^2A' state, formed by $\pi^* \leftarrow \pi$ excitation) is bent, with relatively extended C≡C and C–H bond lengths.[217–219] Laser induced fluorescence measurements of the B–X system and of the B state fluorescence lifetimes return an upper limit value for D_0(CC–H) $\leq 39\,388 \pm 7$ cm^{-1},[220] which is lower than that of the analogous C–H bond in acetylene (D_0(HCC–H) = 46 074 ± 8 cm^{-1} (ref. 15)). The fastest H atoms evident in early PTS studies of C_2H_2 at λ = 193 nm can be attributed to secondary photolysis of the nascent C_2H radicals,[24] and *ab initio* calculations of the PESs for the ground and first few excited states of C_2H along R_{C-H}[217–219] provide some rationale for the spread of electronic states in which the resulting C_2 products are observed.[221]

Propargyl and its fragmentation products. The propargyl (H_2CCCH) radical is the most stable C_3H_3 species and the dominant molecular fragment in the UV photoinduced C–H bond fission of propyne (and allene), as described in Section 2.1. The propargyl radical shows a broad UV absorption peaking at $\lambda \sim 242$ nm,[222] and PTS studies have explored the dissociation dynamics of this radical following excitation at one (242 nm[223] and 248 nm[224]) or several[225] wavelengths within this band. These studies confirm C–H bond fission as the dominant dissociation channel, and that fragmentation occurs following IC to high vibrational levels of the ground state. The identity of the C_3H_2 fragments has not been established definitively; the most translationally excited products imply some formation of the lowest energy cyclopropenylidene (c-C_3H_2) isomer,[223,224] but RRKM calculations have suggested that the quasi-linear triplet propargylene (or propynylidene), HCCCH, isomer should be the dominant C_3H_2 product in any statistically governed dissociation of vibrationally excited ground state propargyl radicals.[226] A recent study of propargyl radical photolysis at 193 nm serves to illustrate some of new opportunities afforded by chirped-pulse mm-wave spectroscopy detection methods. The mm-wave spectrum allows discrimination between (and at least approximate quantitation of) the various C_3H_2 isomers and confirms that H + ^{3}HCCCH products constitute ~80% of the total dissociation yield.[227]

Photofragmentation studies involving the various C_3H_2 isomers are still rare. Propargylene (HCCCH) has a triplet ground state. Anion photodetachment spectroscopy[228] has revealed two low-lying singlet excited states, and confirmed the lower of two triplet excited states identified in earlier matrix isolation spectroscopy studies (with absorption maxima at $\lambda \sim 300$ nm and ~245 nm[229]). Ion imaging studies of the H atoms formed following λ = 250 nm photolysis of propargylene biradicals return an isotropic velocity distribution peaking at low kinetic energies reminiscent of that found in many other systems where dissociation occurs after IC to the ground state PES. In this case, however, complementary non-adiabatic surface hopping calculations suggest that dissociations from excited triplet states also contribute to the measured dissociation yield.[230]

The two carbene isomers, propadienylidene (H_2CCC) and cyclopropenylidene (c-C_3H_2), both have singlet ground states. Features attributable to vibronic levels of the second excited singlet (S_2 or $\tilde{B}^1B_1$) state of c-C_3H_2 have been identified by resonance enhanced multiphoton ionization (REMPI) studies at $\lambda \sim 270$ nm. Ultrafast pump–probe ion yield studies and *ab initio* dynamics simulations both imply fast (<1 ps) non-adiabatic coupling to the S_1 state and thence to the S_0 state, yielding H atoms with a kinetic energy distribution consistent with that expected from the statistical decay of vibrationally excited ground state C_3H_2 radicals.[231] The calculations suggest that the majority co-fragment is c-C_3H, but also reveal some propensity for ring-opening. Time resolved ion yield studies reveal similarly fast excited state decay when exciting the H_2CCC isomer at $\lambda \sim 250$ nm (to its S_3 or $\tilde{C}^1A_1$ state),[232] and the measured Doppler profiles of the H atom fragments are again consistent with IC and subsequent unimolecular decay of vibrationally 'hot' S_0 species.[233]

Vinyl, allyl and heavier homologues. Vinyl (C_2H_3) radicals are formed in the UV photolysis of ethene[56] (Section 2.2) and vinyl halides.[234,235] The electronic absorption spectrum of the vinyl radical shows a structured $\tilde{A}$–$\tilde{X}$ band spanning the region 360–500 nm,[236] attributed to an $n \leftarrow \pi$ promotion, and a more intense, unstructured $\tilde{B}$–$\tilde{X}$ ($\pi^* \leftarrow \pi$) absorption centred at $\lambda \sim 230$ nm.[237] The lowest energy dissociation limit (yielding H + C_2H_2 products) lies at ~12 000 cm^{-1}. Only the ground state of C_2H_3 correlates diabatically with H + C_2H_2(X) products. However, the measured lifetimes of the lowest vibrational levels of the $\tilde{A}^2A''$ state are just a few ps (and these lifetimes decrease further with increasing energy), pointing to the presence of efficient non-adiabatic coupling routes to the ground state PES.[236] Ion imaging studies of the H atom products formed following excitation to several low lying vibrational levels of the $C_2H_3(\tilde{A})$ state confirmed C_2H_2 production[238] and HRA-PTS experiments at λ = 366.2 nm and λ = 327.4 nm showed that the C_2H_2 products are formed with an inverted vibrational population distribution (in the C≡C stretch mode (ν_2), with or without one quantum of the bending mode (ν_4 or ν_5)). The H atom co-fragments associated with these two progressions of peaks show, respectively, preferential parallel and perpendicular recoil anisotropies.[235] *Ab initio* electronic structure plus dynamics calculations identify various non-adiabatic pathways by which photoexcited $\tilde{A}$ state radicals can return to the ground state, the lowest energy of which is promoted by nuclear motions consistent with the vibrational activity observed in the products.[239]

Vinyl radical photodissociation has also been investigated at λ = 243.2 nm, by imaging the H atom products. Excitation at this wavelength populates the $\tilde{B}^2A''$ excited state, at energies above the thresholds for forming an H atom with the vinylidene (H_2CC) radical or with C_2H_2 in its lowest triplet excited state. Image analysis suggests that the former (or, possibly, C_2H_2 molecules with internal energies sufficient that interconversion between the H_2CC and HCCH geometries is facile) is the major molecular photoproduct.[234]

The C_3H_5 radical exists as four isomers: 1-propenyl (CH_3CHCH), 2-propenyl (CH_2CCH_3), cyclo-propyl (c-C_3H_5) and allyl (CH_2CHCH_2). The two propenyl isomers are simply β- and α-CH_3 substituted vinyl radicals. Theory predicts that both will show a similar pattern of excited valence states to that of the allyl radical.[240] PTS studies following excitation of 1-propenyl radicals in the range 224 $\leq \lambda \leq$ 248 nm reveal the formation of H atom products with recoil velocity distributions that are consistent with unimolecular decay to H + C_3H_4 products following IC to the ground state.[241] Accompanying quasi-classical trajectory calculations suggest propyne as the dominant C_3H_4 product, but also suggest that C–C bond fission (yielding CH_3 + C_2H_2 products) is the dominant decay path for the vibrationally 'hot' ground state radicals – in accord with conclusions reached in earlier PTS studies of the λ = 193 nm photolysis of the 1-propenyl radical products from photodissociation of *cis*-1-bromopropene.[242]

Allyl is the simplest hydrocarbon radical with a conjugated π-electron system and, as such, has long been viewed as a benchmark system – for experiment and theory. The allyl radical exhibits diffuse banded absorption in the 410–370 nm region and another UV absorption centred at $\lambda \sim$ 225 nm, and excitations attributed to 3s and 3p Rydberg states have been identified by REMPI spectroscopy.[243] PTS studies following excitation at λ = 351 nm and at λ = 248 nm identified C–H bond fission as the dominant decay channel at both wavelengths,[244] with a minor (~5%) contribution from C–C bond fission at λ = 248 nm.[245] Trajectory calculations, run on an *ab initio* calculated ground state PES at a total energy appropriate for 248 nm photon absorption, reproduce the observed dominance of C–H bond fission and predict allene as the major C_3H_4 product[246] – in accord with the conclusions reached by measuring relative H/D atom yields following photoexcitation of strategically deuterated allyl radicals at λ = 248.2 nm.[247] Three different mechanisms have been proposed as contributors to the observed (minor) yield of C–C bond fission products following excitation at λ = 248 nm – with both C_2H_2 and H_2CC (vinylidene) identified as partners to the CH_3 co-fragment.[246] HRA-PTS studies of the H atom products formed following excitation of allyl to the $\tilde{B}^2A_1(3s)$, $\tilde{C}^2B_2(3p_y)$ and $\tilde{E}^2B_1(p_x)$ excited states (at various wavelengths in the range 216 $\leq \lambda \leq$ 248 nm) serve to reinforce the conclusion that dissociation occurs after IC to the ground state PES.[243] Femtosecond time resolved photoelectron imaging studies of 2-methylallyl radicals following photoexcitation at various wavelengths in the range 236 $\leq \lambda \leq$ 241 nm similarly conclude that the excited state population undergoes rapid IC to the ground state PES.[248]

Studies of the 248 nm photolysis of cyclopentadienyl radicals have identified two major fragmentation channels yielding, respectively, C_3H_3 + C_2H_2 and H + C_5H_4 products with the latter product identified as the ethynylallene isomer.[249] Once again, the deduced product branching ratio and the respective product energy disposals are broadly consistent with fragmentation occurring after IC to the ground state PES.

Substituted unsaturated aliphatic radicals. Relating O with CH_2, the formyl (HCO), acetyl (CH_3CO) and vinoxy (CH_2CHO) radicals are isoelectronic with, respectively, the vinyl, 2-propenyl and allyl radicals. The $\tilde{X}$ and $\tilde{A}$ states of the HCO radical are a Renner–Teller pair,[250] the H–CO bond is weak (D_0(H–CO) = 5083 ± 8 cm^{-1}) and the photodissociation dynamics following excitation at visible wavelengths have been explored by measuring linewidths of the predissociating parent resonances,[251] the energy disposal in the resulting CO products,[252] the recoil anisotropies of the H and CO photofragments,[253] and by velocity map imaging[254] and HRA-PTS studies[255] of the H atom products. The last of these studies provides a particularly clear illustration of quantum interference effects in the decay of vibronically state selected HCO(A) radicals to H + CO(X,*v*,*J*) products.[255] Studies of the energy disposal in the CO products from predissociation of vibrationally state selected HCO($\tilde{X}$) radicals (formed by stimulated emission pumping *via* the $\tilde{B}$ state) have also been reported.[256] The photochemistry of the acetyl radical has received much less attention, but it too shows a broad visible absorption.[257] Theory confirms the low barrier to H_3C–CO bond fission,[258] but the Doppler broadened lineshapes of the H/D atom photofragments measured following (multiphoton) 243 nm excitation of acetone, acetaldehyde and acetic acid have been taken as evidence of (one photon induced) C–H bond fission of the primary acetyl radical photoproducts.[259]

H + CH_2CO (and CH_3 + CO) products have been found following preparation of $\tilde{B}$ state vinoxy (CH_2CHO) radicals by photodetachment of the vinoxide anion at λ = 347 nm.[260] These same product pairs were also identified from the unimolecular decay of highly internally excited vinoxy radicals formed in the photolysis of chloroacetaldehyde at λ = 193 nm[261] and λ = 157 nm.[262] Again, IC to the ground state PES was assumed to precede fragmentation, and theory has identified conical intersections that could facilitate non-adiabatic transfer between the $\tilde{B}$, $\tilde{A}$ and $\tilde{X}$ state PESs.[263] A similar fragmentation mechanism has been invoked to account for the (dominant) CH_3 + CH_2CO and (minor) C_2H_5 + CO product yields and TKER distributions observed when exciting 1- (or i-)methyl-vinoxy (CH_3COCH_2) radicals at λ = 225, 248, and 308 nm.[264]

The methylene amidogen (H_2CN) radical is also isoelectronic with the vinyl radical. TOF measurements of the H atoms formed following photoexcitation of H_2CN in the range 274 $\leq \lambda \leq$ 288 nm reveal a near isotropic recoil velocity distribution and that most of the energy above that required for C–H bond fission is partitioned into internal energy of the HCN co-fragment.[265] *Ab initio* theory confirms that the photoprepared $\tilde{B}^2A_1$ state of H_2CN correlates with an excited state of HCN and that the observed fragmentation proceeds *via* non-adiabatic coupling to the ground state PES.[266]

3.4 Phenyl, benzyl and larger aromatic radicals

As noted in Section 2.3, deep-UV photolysis of benzene yields vibrationally excited phenyl (C_6H_5) radicals that can spontaneously

decay to yield another H atom and a C_6H_4 (*o*-benzyne) fragment. HRA-PTS studies following photolysis of jet-cooled C_6H_5 radicals in the range $215 \leq \lambda \leq 268$ nm – within the $\tilde{B}^2A_1$–$\tilde{X}^2A_1$ ($\pi^* \leftarrow \pi$) absorption system[267] – return isotropic velocity distributions and H atom production rates compatible with C–H bond fission and formation of *o*-C_6H_4 products after IC to the ground state PES.[268] Further support for such a fragmentation mechanism is provided by traditional PTS studies at 193 nm, which identify a (minor) channel yielding C_2H_2 (along with *n*-C_4H_3) products in addition to one or more channels yielding H atom products.[269] Theory suggests that the molecular fragments, and part of the H atom yield formed at these short excitation wavelengths, arise from the unimolecular decay after ring-opening on the ground state PES.[270]

Such behaviour, *i.e.* non-adiabatic coupling to, and subsequent fragmentation on the ground state PES to yield products with branching ratios and energy disposals that are broadly consistent with statistical models of unimolecular decay, appears to be the 'usual' fate of aryl radicals following UV excitation. For example, PTS studies of photodissociation of benzyl ($C_6H_5CH_2$) radicals following excitation in the range $228 \leq \lambda \leq 270$ nm and at $\lambda = 248$ nm identify C–H bond fission as the dominant decay path (with fulvenallene as the predominant co-fragment), with a minor contribution from the rival CH_3 + benzyne product channel.[271,272] Ion imaging studies of the H atoms formed by photolysis of *o*- and *p*-xylyl radicals at wavelengths $\lambda \sim 310$ nm and $\sim$250 nm are similarly consistent with C–H bond fission after IC to the ground state PES.[273] These data all serve to illustrate the extent of isomerisation (ring opening and H atom transfer) that is required after accessing the ground state PES in order to sample the lowest energy fragmentation pathways. But these studies also return H atom formation rates that, whilst still slow, are considerably (one or more orders of magnitude) faster than predicted by RRKM calculations for the fully thermalized ground state radical at the relevant excitation energy.[271,273] Might this be a hint that, even in these larger radicals and over these longer timescales, the decay of the 'hot' ground state species is influenced by the dynamical process(es) by which they are formed? In terms of energy disposal at least, this photophysical behaviour appears to extend to heteroaryl radicals also. The *o*-pyridyl radical is isoelectronic with phenyl, and the recoil velocity distributions of the H atoms formed following excitation of *o*-pyridyl radicals in the range $224 \leq \lambda \leq 246$ nm are consistent with C–H bond fission (yielding cyanovinylacetylene co-fragments) after IC and isomerisation initiated by ring-opening at the C–N bond.[274] Similar data has been reported (and similar conclusions reached) for the photodissociation of *m*-pyridyl radicals following excitation at similar UV wavelengths.[275]

4. Conclusions

Experiment and theory are now revealing many details of the rich photochemistry displayed by hydrocarbon molecules. The UV absorption spectra of the smaller alkynes show resolvable fine structure at long wavelengths, reflecting the fact that the lowest levels of the first $^1\pi\pi^*$ states of these molecules lie below the threshold energy for C–H bond fission. Molecules excited to such levels fluoresce. C–H bond fission sets in upon tuning to higher energies, however, initially by coupling to one or more of the $^3\pi\pi^*$ PESs that correlate to the lowest dissociation products. At yet shorter excitation wavelengths, this ISC channel is overtaken by a $^1\pi\sigma^*$-state mediated C–H bond fission channel, reminiscent of that identified in numerous molecules containing X–H (X = heteroatom) bonds.[7]

The studies of alkenes reported to date reveal very different photofragmentation behaviour. The first excited states again arise *via* $\pi^* \leftarrow \pi$ transitions, but the electron promotion drives torsional motion about what (hitherto) was the C=C bond and facilitates efficient non-adiabatic coupling to the S_0 state. This accounts for the near ubiquitous finding that the photofragmentation of alkenes can be rationalised in terms of the unimolecular decay of highly internally excited S_0 molecules. The singlet state formed by $3s/\sigma^* \leftarrow \pi$ excitation in ethene correlates diabatically with electronically excited C_2H_3 fragments, so any potential rival $^1\pi\sigma^*$-state mediated C–H bond fission channel in alkenes would likely only reveal itself at shorter excitation wavelengths than investigated thus far. Similar considerations apply in the case of the aromatic molecules studied to date, though ISC provides a (relatively) more important non-radiative decay path when exciting at UV wavelengths.

Turning now to the alkanes, the recent studies of methane photophysics conclude that dissociation also occurs after efficient non-adiabatic coupling to the S_0 state. However, at least in the case of CH_4, the nuclear motions that promote the non-adiabatic coupling are closely aligned to the eventual fragmentation coordinate and an IC-driven dissociation thus has many of the dynamical hallmarks traditionally associated with a direct dissociation occurring on a repulsive excited state PES.

Extending such photodynamical studies to larger hydrocarbons will be challenging. These molecules contain just C and H atoms, and multiple C–C and C–H bonds. The parent molecules, and the radical products from C–H bond fission, can often exist in several isomeric forms. Products from the decay of hot S_0 molecules are often formed with sufficient internal energy that they can undergo further unimolecular decay (*i.e.* a triple fragmentation process viewed from the perspective of the photoexcited parent molecule). The primary radical products are also prone to unintended secondary photolysis. Any such secondary dissociation products add to, and potentially confuse the interpretation of, the measured velocity distributions and the yields of the lighter fragments (*e.g.* H atoms, H_2 molecules, *etc.*) that are typically most accessible to experimental study. Such challenges are also present when investigating hydrocarbon radicals, and are compounded by the need to produce a sufficient dense, pure and internally cold source of the radical.

We note some generic thermochemical and spectroscopic differences between hydrocarbon radicals and molecules. The C–H bonds in a hydrocarbon radical (R) are generally 'weaker' than those in the corresponding closed shell hydrocarbon precursor (RH), but the extent of the weakening can be very

system dependent. For example, as shown in Section 3.3, D_0(CC–H) is ~85% that of D_0(HCC–H), whereas the β C–H bond dissociation energy in the vinyl radical is only ~30% that of a C–H bond in ethene. The experimental bond dissociation energies reflect not just the intrinsic 'strength' of the C–H bond of interest, but also the additional stabilization or destabilization of the dissociation products. The big difference in the latter case can be traced to the facts that (i) C–H bond fission in the vinyl radical generates an additional π bond upon forming the product (C_2H_2) and (ii) the C–H bonds in C_2H_2 are stronger due to the sp hybridization. The ground state hydrocarbon radicals have a partially filled HOMO. Electron promotions from (and to) this orbital typically support more valence excited states than in the corresponding closed shell RH molecule. Further, this odd electron will generally have a lower binding energy than that of the electrons in the HOMO of the RH molecule. Thus, the first ionization potential of R will be below that of RH and, more significantly from the viewpoint of the UV spectroscopy, so too will be the energies of the Rydberg states converging to this limit.

This offers one crumb of comfort to those exploring the photofragmentation of hydrocarbon radicals. In many cases, the products from photoinduced C–H bond fission in a hydrocarbon radical will be a closed shell molecule – and thus immune to unintended photochemistry at the UV wavelengths under investigation. Based on the limited available data, the alkyl radicals stand out from most of the other hydrocarbon radicals considered in this study – by yielding some C–H bond fission products with high translational energies and anisotropic recoil velocity distributions consistent with excited state dissociation mediated by the ^{2}n(3s/σ*) PES. For all but the very simplest unsaturated hydrocarbon radicals, in contrast, the dissociation products formed upon photoexcitation, their relative yields, and their translational energy distributions, all appear – at least on a first glance – to be broadly consistent with expectations based on the 'statistical' decomposition of highly vibrationally excited ground state species. But, as noted at several points in this Perspective, there are a sufficient number of niggling inconsistencies with regard to estimated product yields, or product production rate constants, to encourage caution. The fragmentation of highly internally excited ground state radicals (and molecules) should only be expected to display truly 'statistical' characteristics if the internal energy in the 'hot' species has had time to become fully randomised. The internal energy distribution in a species immediately after radiationless transfer to its ground state PES must reflect specific nuclear motions that promote the non-adiabatic coupling, and is thus most unlikely to involve statistical population of all of the energetically accessible vibrational levels. Intramolecular vibrational redistribution, towards this statistical limit, will occur in competition with unimolecular decay, and the relatively probabilities of these processes will be sensitively dependent upon the nuclear motions imprinted during the non-adiabatic coupling and the topography of the ground state PES that the species sample thereafter.

Clearly, there remains a pressing need for further studies – particularly at shorter excitation wavelengths – to test the extent to which the characteristics of fragmentations of 'hot' ground state molecules/radicals formed *via* non-adiabatic coupling from a higher excited state deviate for expectations based on statistics. Fortunately, we can anticipate considerable progress in the near future, given the relentless advances in experimental capability (*e.g.* the increasing availability of intense, short pulse duration, tuneable (V)UV sources for time-resolved pump (photolysis)–probe (*e.g.* universal photoionization) product imaging experiments) and in the accuracy and efficiency of electronic structure methods and in the treatment of non-adiabatic excited state dynamics. Determining and explaining the dynamics of a specific photofragmentation channel is a fascinating and rewarding intellectual challenge, but we should not forget that, in many cases, there is still a need to establish reliable branching ratios (quantum yields) for competing fragmentation channels and how these vary with photolysis wavelength. Such information is a key yet, in many cases still poorly determined, part of the input to models of the atmospheres of the outer planets in our solar system and beyond.[276]

Conflicts of interest

There are no conflicts to declare.

Appendix

The ground state minimum energy geometries were optimised using Møller–Plesset second order perturbation theory (MP2)[277] coupled to Dunning's cc-pVDZ basis set.[278] Unrelaxed, rigid-body potential energy profiles were constructed using complete-active space second order perturbation theory (CASPT2),[279,280] coupled to Dunning's aug-cc-pVDZ basis set. The CASPT2 calculations were based on a state-averaged complete-active space self-consistent field (SA-CASSCF) reference wavefunction. An imaginary level shift of 0.5 E_H was used to aid convergence and to mitigate intruder state effects.

The active space used was species specific. C_{2v} symmetry and a full-valence active space was used for the CH, CH_2 and CH_3 radicals. For CH_4 and HCHO, C_s symmetry was used. The CH_4 calculations used an (8,8) active space (*i.e.* 8 electrons in 8 orbitals, six of A′ and two of A″ symmetry) while those for HCHO used a (6,5) active space (3 A′ and 2 A″ orbitals). The C_2H_2 calculations used C_{2v} symmetry and a (10,8) active space comprising 4 A_1, 2 B_1 and 2 B_2 orbitals, while those for C_2H_4 assumed C_s symmetry and used a (4,4) active space (2 A′ and 2A″ orbitals). For benzene, C_s symmetry and an active space of 8 electrons in 8 orbitals (6 A″ and 2 A′) was used. The optimisations of the conical intersections for C_2H_2 and benzene used, respectively, (2,2) and (6,6) active spaces. These calculations made use of the 6-31G(d) basis set. All optimisations were carried out in Gaussian 09[281] whilst the potential energy scans were performed in MOLPRO 2010.1.[12]

The MECIs shown in Fig. 5 were obtained by performing the seam model function (SMF)/single-component artificial force induced reaction (SC-AFIR) method, with spin-flip time-dependent

density functional theory (SF-TDDFT), as implemented in a developmental version of the global reaction route mapping program (GRRM).[153–156] The searches were started from ground state equilibrium structures, using the BHHLYP functional and 6-31G(d) basis set.

Additional outputs that underpin the *ab initio* calculations reported in this paper have been placed in the University of Bristol's research data repository and can be accessed using the following DOI: 10.5523/bris.3tm9tsqgl5w3n2bdykoltp78q9.

Acknowledgements

MNRA is grateful to the Engineering and Physical Sciences Research Council for funding through a Programme Grant (EP/L005913). RAI is grateful to Prof. Satoshi Maeda and Dr Yu. Harabuchi for access to computational resources and a development version of the GRRM code and helpful discussions. JSZ acknowledges the support from the US National Science Foundation (NSF CHE-1566636).

References

1 J. Cui, R. V. Yelle, V. Vuitton, J. H. Waite, W. T. Kasprzak, D. A. Gell., H. B. Niemann, I. C. F. Muller-Wodarg, N. Borggren, G. G. Fletcher, E. L. Patrick, E. Raaen and B. A. Magee, *Icarus*, 2009, **200**, 581–615.
2 V. G. Kunde, A. C. Aikin, R. A. Hanel, D. E. Jennings, W. C. Maguire and R. E. Samuelson, *Nature*, 1981, **292**, 686–688.
3 V. A. Krasnopolsky, *Icarus*, 2009, **201**, 226–256.
4 J. C. Loison, E. Hebrard, M. Dobrijevic, K. M. Hickson, F. Caralp, V. Hue, G. Gronoff, O. Venot and Y. Benilan, *Icarus*, 2015, **247**, 218–247.
5 Y. L. Yung and W. B. DeMore, *Photochemistry of Planetary Atmospheres*, Oxford University Press, 1999.
6 A. L. Sobolewski, W. Domcke, C. Dedonder-Lardeux and C. Jouvet, *Phys. Chem. Chem. Phys.*, 2002, **4**, 1093–1100.
7 M. N. R. Ashfold, G. A. King, D. Murdock, M. G. D. Nix, T. A. A. Oliver and A. G. Sage, *Phys. Chem. Chem. Phys.*, 2010, **12**, 1218–1238.
8 G. M. Roberts and V. G. Stavros, *Chem. Sci.*, 2014, **5**, 1698–1722.
9 M. N. R. Ashfold, D. Murdock and T. A. A. Oliver, *Annu. Rev. Phys. Chem.*, 2017, **68**, 63–82.
10 A. G. Sage, T. A. A. Oliver, D. Murdock, M. B. Crow, G. A. D. Ritchie, J. N. Harvey and M. N. R. Ashfold, *Phys. Chem. Chem. Phys.*, 2011, **13**, 8075–8093.
11 M. N. R. Ashfold, M. Bain, C. S. Hansen, R. A. Ingle, T. N. V. Karsili, B. Marchetti and D. Murdock, *J. Phys. Chem. Lett.*, 2017, **8**, 3440–3451.
12 H. J. Werner, P. J. Knowles, G. Knizia, F. R. Manby, M. Schütz, P. Celani, W. Győrffy, D. Kats, T. Korona and R. Lindh, *et al.*, *MOLPRO, version 2015.1, A Package of ab initio Programs*, see http://www.molpro.net.
13 See, for example, T. E. Sharp, *At. Data Nucl. Data Tables*, 1971, **2**, 119–169.
14 T. Suzuki and N. Hashimoto, *J. Chem. Phys.*, 1999, **110**, 2042–2050.
15 D. H. Mordaunt and M. N. R. Ashfold, *J. Chem. Phys.*, 1994, **101**, 2630–2631.
16 N. Yamakita, S. Iwamoto and S. Tsuchiya, *J. Phys. Chem. A*, 2003, **107**, 2597–2605.
17 P. B. Changala, J. H. Baraban, A. J. Merer and R. W. Field, *J. Chem. Phys.*, 2015, **143**, 084310.
18 D. H. Mordaunt, M. N. R. Ashfold, R. N. Dixon, P. Löffler, L. Schnieder and K. H. Welge, *J. Chem. Phys.*, 1998, **108**, 519–526.
19 J. Jiang, C. A. Saladrigas, T. J. Erickson, C. L. Keenan and R. W. Field, *J. Chem. Phys.*, 2018, **149**, 174309.
20 Q. Cui and K. Morokuma, *Chem. Phys. Lett.*, 1997, **272**, 319–327.
21 R. P. Schmid, T. Arusi-Parpar, R.-J. Li, I. Bar and S. Rosenwaks, *J. Chem. Phys.*, 1997, **107**, 385–391.
22 I. Bar and S. Rosenwaks, *Mol. Phys.*, 2012, **110**, 2673–2686.
23 J. Zhang, C. W. Riehn, M. Dulligan and C. Wittig, *J. Chem. Phys.*, 1995, **103**, 6815–6818.
24 B. A. Balko, J. Zhang and Y. T. Lee, *J. Chem. Phys.*, 1991, **94**, 7958–7966.
25 Y. Zhang, K. Yuan, S. Yu, D. H. Parker and X. Yang, *J. Chem. Phys.*, 2010, **133**, 014307.
26 J.-H. Wang, Y.-T. Hsu and K. Liu, *J. Phys. Chem. A*, 1997, **101**, 6593–6602.
27 P. Löffler, D. Lacombe, A. Ross, E. Wrede, L. Schnieder and K. H. Welge, *Chem. Phys. Lett.*, 1996, **252**, 304–310.
28 P. Löffler, E. Wrede, L. Schnieder, J. B. Halpern, W. M. Jackson and K. H. Welge, *J. Chem. Phys.*, 1998, **109**, 5231–5246.
29 S. Boyé, A. Campos, S. Douin, C. Fellows, D. Gauyacq, N. Shafizadeh, Ph. Halvick and M. Boggio-Pasqua, *J. Chem. Phys.*, 2002, **116**, 8843–8855.
30 R. E. Bandy, C. Lakshminarayan, R. K. Frost and T. S. Zwier, *Science*, 1992, **258**, 1630–1633.
31 R. Silva, W. K. Gichuhi, C. Huang, M. B. Doyle, V. V. Kislov, A. M. Mebel and A. G. Suits, *PNAS*, 2008, **105**, 12713–12718.
32 S. R. Yu, S. Su, Y. W. Zhang, D. X. Dai, K. J. Yuan and X. M. Yang, *J. Chem. Phys.*, 2013, **139**, 124307.
33 H. Z. Wang, S. R. Yu, S. Su, D. X. Dai, K. J. Yuan and X. M. Yang, *J. Phys. Chem. A*, 2015, **119**, 11313–11319.
34 S. Satyapal and R. Bersohn, *J. Phys. Chem.*, 1991, **95**, 8004–8006.
35 C.-K. Ni, J. D. Huang, Y. T. Chen, A. H. Kung and W. M. Jackson, *J. Chem. Phys.*, 1998, **110**, 3320–3325.
36 W. Sun, K. Yokoyama, J. C. Robinson, A. G. Suits and D. M. Neumark, *J. Chem. Phys.*, 1999, **110**, 4363–4368.
37 S. Ghosh, A. K. Rauta and B. Maiti, *Phys. Chem. Chem. Phys.*, 2016, **18**, 8219–8227.
38 R. H. Qadiri, E. J. Feltham, E. E. H. Cottrill, N. Taniguchi and M. N. R. Ashfold, *J. Chem. Phys.*, 2002, **116**, 906–912.
39 R. H. Qadiri, E. J. Feltham, N. H. Nahler, R. P. Garcia and M. N. R. Ashfold, *J. Chem. Phys.*, 2003, **119**, 12842–12851.
40 K. Seki and H. Okabe, *J. Phys. Chem.*, 1992, **96**, 3345–3349.
41 X. Chen, Y. Ganot, I. Bar and S. Rosenwaks, *J. Chem. Phys.*, 2000, **113**, 5134–5137.

42 W. M. Jackson, D. S. Anex, R. E. Continetti, B. A. Balko and Y. T. Lee, *J. Chem. Phys.*, 1991, **95**, 7327–7336.
43 J. C. Robinson, N. E. Sveum, S. J. Goncher and D. M. Neumark, *Mol. Phys.*, 2005, **103**, 1765–1783.
44 S. Harich, J. J. Lin, Y. T. Lee and X. M. Yang, *J. Chem. Phys.*, 2000, **112**, 6656–6665.
45 K. Alnama, S. Boyé-Péronne, S. Douin, F. Innocenti, J. O'Reilly, A.-L. Roche, N. Shafizadeh, L. Zuin and D. Gauyacq, *J. Chem. Phys.*, 2007, **126**, 044304.
46 R. Silva, W. K. Gichuhi, V. V. Kislov, A. Landera, A. M. Mebel and A. G. Suits, *J. Phys. Chem. A*, 2009, **113**, 11182–11186.
47 K. Seki, M. Q. He, R. Z. Liu and H. Okabe, *J. Phys. Chem.*, 1996, **100**, 5349–5353.
48 R. Eng, T. Carrington, C. H. Dugan, S. V. Filseth and C. M. Sadowski, *Chem. Phys.*, 1987, **113**, 119–130.
49 J. Z. Guo, R. Eng, T. Carrington and S. V. Filseth, *J. Chem. Phys.*, 2000, **112**, 8904–8909.
50 G. P. Morley, I. R. Lambert, M. N. R. Ashfold, K. N. Rosser and C. M. Western, *J. Chem. Phys.*, 1992, **97**, 3157–3165.
51 P. A. Cook, S. R. Langford, M. N. R. Ashfold and R. N. Dixon, *J. Chem. Phys.*, 2000, **113**, 994–1004.
52 C. R. Bucher and K. K. Lehmann, *Chem. Phys. Lett.*, 1998, **294**, 173–180.
53 G. A. West and M. J. Berry, *J. Chem. Phys.*, 1974, **61**, 4700–4716.
54 A. J. Merer and R. S. Mulliken, *Chem. Rev.*, 1969, **69**, 639–656.
55 K. Alnama, S. Boyé-Péronne, A.-L. Roche and D. Gauyacq, *Mol. Phys.*, 2007, **105**, 1743–1756.
56 B. A. Balko, J. Zhang and Y. T. Lee, *J. Chem. Phys.*, 1992, **97**, 935–942.
57 J. J. Lin, D. W. Hwang, Y. T. Lee and X.-M. Yang, *J. Chem. Phys.*, 1998, **109**, 2979–2982.
58 J. J. Lin, C. C. Wang, Y. T. Lee and X. Yang, *J. Chem. Phys.*, 2000, **113**, 9668–9677.
59 S.-H. Lee, Y. T. Lee and X. Yang, *J. Chem. Phys.*, 2004, **120**, 10983–10991.
60 S.-H. Lee, Y.-C. Lee and Y. T. Lee, *J. Phys. Chem. A*, 2006, **110**, 2337–2344.
61 K. Alnama, S. Boyé, S. Douin, F. Innocenti, J. O'Reilly, A.-L. Roche, N. Shafizadeh, L. Zuin and D. Gauyacq, *Phys. Chem. Chem. Phys.*, 2004, **6**, 2093–2100.
62 A. Viel, R. P. Krawczyk, U. Manthe and W. Domcke, *J. Chem. Phys.*, 2004, **120**, 11000–11010.
63 M. Barbatti, J. Paier and H. Lischka, *J. Chem. Phys.*, 2004, **121**, 11614–11624.
64 T. Mori, W. J. Glover, M. S. Schuurman and T. J. Martinez, *J. Phys. Chem. A*, 2012, **116**, 2808–2818.
65 T. K. Allison, H. Tao, W. J. Glover, T. W. Wright, A. M. Stooke, C. Khurmi, J. van Tilborg, Y. Liu, R. W. Falcone, T. J. Martinez and A. Belkacem, *J. Chem. Phys.*, 2012, **136**, 124317.
66 B. Sellner, M. Barbatti, T. Müller, W. Domcke and H. Lischka, *Mol. Phys.*, 2013, **111**, 2439–2450.
67 K. Kosma, S. A. Trushin, W. Fuss and W. E. Schmid, *J. Phys. Chem. A*, 2008, **112**, 7514–7529.
68 E. G. Champenois, N. H. Shivaram, T. W. Wright, C.-S. Yang, A. Belkacem and J. P. Cryan, *J. Chem. Phys.*, 2016, **144**, 014303.
69 T. Kobayashi, T. Horio and T. Suzuki, *J. Phys. Chem. A*, 2015, **119**, 9518–9523.
70 E. M. Evleth and A. Sevin, *J. Am. Chem. Soc.*, 1981, **103**, 7414–7422.
71 G. Wu, A. E. Boguslavskiy, O. Schalk, M. S. Schuurman and A. Stolow, *J. Chem. Phys.*, 2011, **135**, 164309.
72 G. M. P. Just, B. Negru, D. Park and D. M. Neumark, *Phys. Chem. Chem. Phys.*, 2012, **14**, 675–680.
73 S.-H. Lee, Y.-Y. Lee, Y. T. Lee and X. M. Yang, *J. Chem. Phys.*, 2003, **119**, 827–838.
74 S.-H. Lee, Y. T. Lee and X. M. Yang, *J. Chem. Phys.*, 2004, **120**, 10992–10999.
75 S.-H. Lee and Y. T. Lee, *Chem. Phys. Lett.*, 2004, **395**, 311–315.
76 C.-H. Chin and S.-H. Lee, *J. Chem. Phys.*, 2012, **136**, 024308.
77 D. R. Cyr and C. C. Hayden, *J. Chem. Phys.*, 1996, **104**, 771–774.
78 V. Blanchet, M. Z. Zgierski, T. Seidemann and A. Stolow, *Nature*, 1999, **401**, 52–54.
79 F. Assenmacher, M. Gutmann, G. Höhlneicher, V. Stert and W. Radloff, *Phys. Chem. Chem. Phys.*, 2001, **3**, 2981–2982.
80 W. Fuss, W. E. Schmid and S. A. Trushin, *Chem. Phys. Lett.*, 2001, **342**, 91–98.
81 A. Makida, H. Igarashi, T. Fujiwara, T. Sekikawa, Y. Harabuchi and T. Taketsugu, *J. Phys. Chem. Lett.*, 2014, **5**, 1760–1765.
82 J. C. Robinson, S. A. Harris, W. Z. Sun, N. E. Sveum and D. M. Neumark, *J. Am. Chem. Soc.*, 2002, **124**, 10211–10224.
83 M. Olivucci, J. N. Ragazos, F. Bernardi and M. A. Robb, *J. Am. Chem. Soc.*, 1993, **115**, 3710–3721.
84 A. Komainda, B. Ostojic and H. Köppel, *J. Phys. Chem. A*, 2013, **117**, 8782–8793.
85 B. G. Levine and T. J. Martinez, *J. Phys. Chem. A*, 2009, **113**, 12815–12824.
86 T. S. Kuhlman, W. J. Glover, T. Mori, T. Møller and T. J. Martinez, *Faraday Discuss.*, 2012, **157**, 193–212.
87 O. Schalk, A. E. Boguslavskiy and A. Stolow, *J. Phys. Chem. A*, 2010, **114**, 4058–4064.
88 H. L. Tao, B. G. Levine and T. J. Martinez, *J. Phys. Chem. A*, 2009, **113**, 13656–13662.
89 M. Garavelli, C. S. Page, P. Celani, M. Olivucci, W. E. Schmid, S. A. Trushin and W. Fuss, *J. Phys. Chem. A*, 2001, **105**, 4458–4469.
90 K. Kosma, S. A. Trushin, W. Fuss and W. E. Schmid, *Phys. Chem. Chem. Phys.*, 2009, **11**, 172–181.
91 S. Adachi, M. Sato and T. Suzuki, *J. Phys. Chem. Lett.*, 2015, **6**, 343–346.
92 C. C. Pemberton, Y. Zhang, K. Saita, A. Kirrander and P. M. Weber, *J. Phys. Chem. A*, 2015, **119**, 8832–8845.
93 M. P. Minitti, J. M. Budarz, A. Kirrander, J. S. Robinson, D. Ratner, T. J. Lane, D. Zhu, J. M. Glownia, M. Kozina, H. T. Lemke, M. Sikorski, Y. Feng, S. Nelson, K. Saita, B. Stankus, T. Northey, J. B. Hastings and P. M. Weber, *Phys. Rev. Lett.*, 2015, **114**, 255501.

94 O. Schalk, T. Geng, T. Thompson, N. Baluyot, R. D. Thomas, E. Tapavicza and T. Hansson, *J. Phys. Chem. A*, 2016, **120**, 2320–2329.
95 A. R. Attar, A. Bhattacherjee, C. D. Pemmaraju, K. Schnorr, K. D. Closser, D. Prendergast and S. R. Leone, *Science*, 2017, **356**, 54–58.
96 J. Giegerich and I. Fischer, *Phys. Chem. Chem. Phys.*, 2013, **15**, 13162–13168.
97 I. A. Ramphal, M. Shapero, C. Halbach-Morris and D. M. Neumark, *Phys. Chem. Chem. Phys.*, 2017, **19**, 29305–29314.
98 N. Hobday, M. S. Quinn, K. Nauta, D. U. Andrews, M. J. T. Jordan and S. H. Kable, *J. Phys. Chem. A*, 2013, **117**, 12091–12103.
99 W. S. Hopkins, H.-P. Loock, B. Cronin, M. G. D. Nix, A. L. Devine, R. N. Dixon and M. N. R. Ashfold, *J. Chem. Phys.*, 2007, **127**, 064301.
100 M. J. Dulligan, M. F. Tuchler, J. Zhang, A. Kolessov and C. Wittig, *Chem. Phys. Lett.*, 1997, **276**, 84–91.
101 W. S. Hopkins, H.-P. Loock, B. Cronin, M. G. D. Nix, A. L. Devine, R. N. Dixon, M. N. R. Ashfold, H.-M. Yin, S. J. Rowling, A. Büll and S. H. Kable, *J. Phys. Chem. A*, 2008, **112**, 9283–9289.
102 P. Zhang, S. Maeda, K. Morokuma and B. J. Braams, *J. Chem. Phys.*, 2009, **130**, 114304.
103 D. Townsend, S. A. Lahankar, S. K. Lee, S. D. Chambreau, A. G. Suits, X. Zhang, J. Rheinecker, L. B. Harding and J. M. Bowman, *Science*, 2004, **306**, 1158–1161.
104 M. S. Quinn, D. U. Andrews, K. Nauta, M. J. T. Jordan and S. H. Kable, *J. Chem. Phys.*, 2017, **147**, 013935.
105 S. Gomez-Carrasco, T. Muller and H. Köppel, *J. Phys. Chem. A*, 2010, **114**, 11436–11449.
106 K. L. K. Lee, M. S. Quinn, A. T. Maccarone, K. Nauta, P. L. Houston, S. A. Reid, M. J. T. Jordan and S. H. Kable, *Chem. Sci.*, 2014, **5**, 4633–4638.
107 H. K. Li, P. Y. Tsai, K. C. Hung, T. Kasai and K. C. Lin, *J. Chem. Phys.*, 2015, **142**, 041101.
108 B. W. Toulson, K. M. Kapnas, D. A. Fishman and C. Murray, *Phys. Chem. Chem. Phys.*, 2017, **19**, 14276–14288.
109 P. Morajkar, A. Bossolasco, C. Schoemaecker and C. Fittschen, *J. Chem. Phys.*, 2014, **140**, 214308.
110 Y. C. Han, P. Y. Tsai, J. M. Bowman and K. C. Lin, *Phys. Chem. Chem. Phys.*, 2017, **19**, 18628–18634.
111 L. Rubio-Lago, G. A. Amaral, A. Arregui, J. G. Izquierdo, F. Wang, D. Zaouris, T. N. Kitsopoulos and L. Bañares, *Phys. Chem. Chem. Phys.*, 2007, **9**, 6123–6127.
112 T. Y. Kang, S. W. Kang and H. L. Kim, *Chem. Phys. Lett.*, 2007, **434**, 6–10.
113 S.-H. Lee, *J. Chem. Phys.*, 2009, **131**, 174312.
114 P. Y. Tsai, H. K. Li, T. Kasai and K. C. Lin, *Phys. Chem. Chem. Phys.*, 2015, **17**, 23112–23120.
115 S.-H. Jen and I.-C. Chen, *J. Chem. Phys.*, 1999, **111**, 8448–8453.
116 B. M. Haas, T. K. Minton, P. Felder and J. R. Huber, *J. Phys. Chem.*, 1991, **95**, 5149–5159.
117 C. Chaudhuri and S. H. Lee, *Phys. Chem. Chem. Phys.*, 2011, **13**, 7312–7321.
118 C.-H. Chin, C. Chaudhuri and S.-H. Lee, *J. Chem. Phys.*, 2011, **135**, 044301.
119 T. W. R. Hancock and R. N. Dixon, *J. Chem. Soc., Faraday Trans.*, 1997, **93**, 2707–2719.
120 C. L. Reed, M. Kono, S. R. Langford, R. N. Dixon and M. N. R. Ashfold, *J. Chem. Soc., Faraday Trans.*, 1997, **93**, 2721–2729.
121 S. H. Lee, C.-Y. Wu, S.-K. Yang and Y.-P. Lee, *J. Chem. Phys.*, 2005, **123**, 074326.
122 C. Maul, C. Dietrich, T. Haas, K.-H. Gericke, H. Tachikawa, S. R. Langford, M. Kono, C. L. Reed, R. N. Dixon and M. N. R. Ashfold, *Phys. Chem. Chem. Phys.*, 1999, **1**, 767–772.
123 H. Tachikawa, *Phys. Chem. Chem. Phys.*, 1999, **1**, 2675–2679.
124 W.-H. Fang and R.-Z. Liu, *J. Chem. Phys.*, 2001, **115**, 5411–5417.
125 E. A. Wade, H. Clauberg, S. K. Kim, A. Mellinger and C. B. Moore, *J. Phys. Chem. A*, 1997, **101**, 732–739.
126 J. Liu, F. Y. Wang, H. Wang, B. Jiang and X. M. Yang, *J. Chem. Phys.*, 2005, **122**, 104309.
127 G. T. Fujimoto, M. E. Umstead and M. C. Lin, *Chem. Phys.*, 1982, **65**, 197–203.
128 E. J. Feltham, R. H. Qadiri, E. E. H. Cottrill, P. A. Cook, J. P. Cole, G. G. Balint-Kurti and M. N. R. Ashfold, *J. Chem. Phys.*, 2003, **119**, 6017–6031.
129 Y. Liu, J. K. Yu, X. R. Huang and C. C. Sun, *J. Chem. Phys.*, 2006, **125**, 044311.
130 H. Y. Xiao, S. Maeda and K. Morokuma, *J. Phys. Chem. A*, 2013, **117**, 7001–7008.
131 I. C. Lu, S. H. Lee, Y. T. Lee and X. M. Yang, *J. Chem. Phys.*, 2006, **124**, 024324.
132 C.-K. Ni and Y. T. Lee, *Int. Rev. Phys. Chem.*, 2004, **23**, 187–218.
133 R. J. Longfellow, D. B. Moss and C. S. Parmenter, *J. Phys. Chem.*, 1998, **92**, 5438–5449.
134 T. J. Penfold, R. Spesyvtsev, O. M. Kirkby, R. S. Minns, D. S. N. Parker, H. H. Fielding and G. A. Worth, *J. Chem. Phys.*, 2012, **137**, 204310.
135 A. Yokoyama, X. Zhao, E. J. Hintsa, R. E. Continetti and Y. T. Lee, *J. Chem. Phys.*, 1990, **92**, 4222–4233.
136 A. M. Mebel, S. H. Lin, X. M. Yang and Y. T. Lee, *J. Phys. Chem. A*, 1997, **101**, 6781–6789.
137 C. K. Lin, C. L. Huang, J. C. Jiang, A. H. H. Chang, Y. T. Lee, S. H. Lin and C. K. Ni, *J. Am. Chem. Soc.*, 2002, **124**, 4068–4075.
138 C. L. Huang, J. C. Jiang, A. H. H. Chang, Y. T. Lee and C. K. Ni, *J. Phys. Chem. A*, 2003, **107**, 4019–4024.
139 C. L. Huang, J. C. Jiang, S. H. Lin, Y. T. Lee and C. K. Ni, *J. Chem. Phys.*, 2002, **116**, 7779–7782.
140 C. L. Huang, J. C. Jiang, Y. T. Lee and C. K. Ni, *J. Chem. Phys.*, 2002, **117**, 7034–7040.
141 D. H. Mordaunt, I. R. Lambert, G. P. Morley, M. N. R. Ashfold, R. N. Dixon, L. Schnieder and K. H. Welge, *J. Chem. Phys.*, 1993, **98**, 2054–2065.
142 A. J. R. Heck, R. N. Zare and D. W. Chandler, *J. Chem. Phys.*, 1996, **104**, 4019–4030.

143 J.-H. Wang and K. Liu, *J. Chem. Phys.*, 1998, **109**, 7105–7112.
144 J.-H. Wang, K. Liu, Z. Y. Min, H. M. Su, R. Bersohn, J. Preses and J. Z. Larese, *J. Chem. Phys.*, 2000, **113**, 4146–4152.
145 P. A. Cook, M. N. R. Ashfold, Y.-J. Lee, K.-H. Jung, S. Harich and X. Yang, *Phys. Chem. Chem. Phys.*, 2001, **3**, 1848–1860.
146 Y. W. Zhang, K. J. Yuan, S. R. Yu and X. M. Yang, *J. Phys. Chem. Lett.*, 2010, **1**, 475–479.
147 F. Z. Chen and C. Y. R. Wu, *J. Quant. Spectrosc. Radiat. Transfer*, 2004, **85**, 195–209.
148 B. Gans, S. Boyé-Péronne, M. Broquier, M. Delsaut, S. Douin, C. E. Fellows, P. Halvick, J.-C. Loison, R. R. Lucchese and D. Gauyacq, *Phys. Chem. Chem. Phys.*, 2011, **13**, 8140–8152.
149 L. C. Lee and C. C. Chiang, *J. Chem. Phys.*, 1983, **78**, 688–691.
150 A. M. Mebel, S.-H. Lin and C.-H. Chang, *J. Chem. Phys.*, 1997, **106**, 2612–2620.
151 R. van Harrevelt, *J. Chem. Phys.*, 2006, **125**, 124302.
152 M. D. Lodriguito, G. Lendvay and G. C. Schatz, *J. Chem. Phys.*, 2009, **131**, 224320.
153 S. Maeda, K. Ohno and K. Morokuma, *Phys. Chem. Chem. Phys.*, 2013, **15**, 3683–3701.
154 S. Maeda, T. Taketsugu and K. Morokuma, *J. Comput. Chem.*, 2014, **35**, 166–173.
155 S. Maeda, T. Taketsugu, K. Ohno and K. Morokuma, *J. Am. Chem. Soc.*, 2015, **137**, 3433–3445.
156 S. Maeda, Y. Osada, Y. Harabuchi, T. Taketsugu, K. Morokuma and K. Ohno, *GRRM, a developmental version*, Hokkaido University, Sapporo, 2015.
157 D. H. Mordaunt, M. N. R. Ashfold and R. N. Dixon, *J. Chem. Phys.*, 1996, **104**, 6460–6471.
158 A. V. Demyanenko, V. Dribinski, H. Reisler, H. Meyer and C. X. W. Qian, *J. Chem. Phys.*, 1999, **111**, 7383–7396.
159 R. J. Buenker and S. D. Peyerimhoff, *Chem. Phys.*, 1975, **8**, 56–67.
160 U. Jacovella, C. J. Stein, M. Grütter, L. Freitag, C. Lauzin, M. Reiher and F. Merkt, *Phys. Chem. Chem. Phys.*, 2018, **20**, 1072–1081.
161 H. Okabe and J. R. McNesby, *J. Chem. Phys.*, 1961, **34**, 668–669.
162 W. M. Jackson, R. J. Price II, D. D. Xu, J. D. Wrobel, M. Ahmed, D. S. Peterka and A. G. Suits, *J. Chem. Phys.*, 1998, **109**, 4703–4706.
163 S. M. Wu, J. J. Lin, Y. T. Lee and X. Yang, *J. Chem. Phys.*, 2000, **112**, 8027–8037.
164 A. K. Rauta and B. Maiti, *J. Chem. Phys.*, 2018, **149**, 044308.
165 S. M. Wu, J. J. Lin, Y. T. Lee and X. Yang, *J. Phys. Chem. A*, 2000, **104**, 7189–7199.
166 C. C. Wang, Y. T. Lee, J. J. Lin, J. Shu., Y.-Y. Lee and X. Yang, *J. Chem. Phys.*, 2002, **117**, 153–160.
167 K. Tonokura, Y. Matsumi and M. Kawasaki, *J. Chem. Phys.*, 1991, **95**, 5065–5071.
168 K. Tonokura, Y. Mo, Y. Matsumi and M. Kawasaki, *J. Phys. Chem.*, 1992, **96**, 6688–6693.
169 R. A. Brownsword, M. Hillenkamp, T. Laurent, R. K. Vatsa, H. R. Volpp and J. Wolfrum, *J. Chem. Phys.*, 1997, **106**, 1359–1366.
170 G. Amaral, K. S. Xu and J. S. Zhang, *J. Phys. Chem. A*, 2001, **105**, 1115–1120.
171 M. Lucas, Y. L. Liu, R. Bryant, J. Minor and J. S. Zhang, *Chem. Phys. Lett.*, 2015, **619**, 18–22.
172 A. Kalemos, A. Mavridis and A. Metropoulos, *J. Chem. Phys.*, 1999, **111**, 9536–9548.
173 E. F. van Dishoeck, *J. Chem. Phys.*, 1987, **86**, 196–214.
174 R. A. Beärda, M. C. van Hemert and E. F. van Dishoeck, *J. Chem. Phys.*, 1992, **97**, 8240–8249.
175 G. J. Kroes, E. F. van Dishoeck, R. A. Beärda and M. C. van Hemert, *J. Chem. Phys.*, 1993, **99**, 228–236.
176 R. A. Beärda, G. J. Kroes, M. C. van Hemert, B. Heumann, R. Schinke and E. F. van Dishoeck, *J. Chem. Phys.*, 1994, **100**, 1113–1127.
177 R. A. Beärda, M. C. van Hemert and E. F. van Dishoeck, *J. Chem. Phys.*, 1995, **102**, 8930–8941.
178 G.-J. Kroes, M. C. van Hemert, G. D. Billing and D. Neuhauser, *J. Chem. Phys.*, 1997, **107**, 5757–5770.
179 B. Bohn and F. Stuhl, *J. Chem. Phys.*, 1995, **102**, 8842–8845.
180 G. Herzberg, *Proc. R. Soc. London*, 1961, **262**, 291–317.
181 G. R. Wu, B. Jiang, Q. Ran, J. H. Zhang, S. A. Harich and X. M. Yang, *J. Chem. Phys.*, 2004, **120**, 2193–2198.
182 S. G. Westre, P. B. Kelly, Y. P. Zhang and L. D. Ziegler, *J. Chem. Phys.*, 1991, **94**, 270–276.
183 S. H. S. Wilson, J. D. Howe, K. N. Rosser, M. N. R. Ashfold and R. N. Dixon, *Chem. Phys. Lett.*, 1994, **227**, 456–460.
184 S. W. North, D. A. Blank, P. M. Chu and Y. T. Lee, *J. Chem. Phys.*, 1995, **102**, 792–798.
185 S. M. Poullian, D. V. Chicharro, A. Zanchet, M. G. Gonzalez, L. Rubio-Lago, M. L. Senent, A. Garcia-Vela and L. Bañares, *Phys. Chem. Chem. Phys.*, 2016, **18**, 17054–17061.
186 H. T. Yu, A. Sevin, E. Kassab and E. M. Evleth, *J. Chem. Phys.*, 1984, **80**, 2049–2059.
187 A. Zanchet, L. Bañares, M. L. Senent and A. Garcia-Vela, *Phys. Chem. Chem. Phys.*, 2016, **18**, 33195–33203.
188 G. Amaral, K. S. Xu and J. S. Zhang, *J. Chem. Phys.*, 2001, **114**, 5164–5169.
189 M. Steinbauer, J. Giegerich, K. H. Fischer and I. Fischer, *J. Chem. Phys.*, 2012, **137**, 014303.
190 A. S. Zyubin, A. M. Mebel and S. H. Lin, *Chem. Phys. Lett.*, 2000, **323**, 441–447.
191 A. Sevin, H. T. Yu and E. M. Evleth, *THEOCHEM*, 1983, **13**, 163–178.
192 J. M. Hostettler, A. Bach and P. Chen, *J. Chem. Phys.*, 2009, **130**, 034303.
193 A. Matsugi, *J. Phys. Chem. Lett.*, 2013, **4**, 4237–4240.
194 J. Giegerich and I. Fischer, *J. Chem. Phys.*, 2015, **142**, 044304.
195 Y. Song, X. F. Zheng, W. D. Zhou, M. Lucas and J. S. Zhang, *J. Chem. Phys.*, 2015, **142**, 224306.
196 Z. G. Wang, M. G. Matthews and B. Koplitz, *J. Phys. Chem.*, 1995, **99**, 6913–6916.
197 G. Sun, Y. Song and J. S. Zhang, *Chin. J. Chem. Phys.*, 2018, **31**, 439–445.

198 W. R. Stevens, S. H. Walker, N. S. Shuman and T. Baer, *J. Phys. Chem. A*, 2010, **114**, 804–810.
199 J. A. Blush and P. Chen, *J. Chem. Phys.*, 1993, **98**, 3557–3559.
200 J. Pacansky, W. Koch and M. D. Miller, *J. Am. Chem. Soc.*, 1991, **113**, 317–328.
201 B. Noller, R. Maksimenka, I. Fischer, M. Armone, B. Engels, C. Alcaraz, L. Poisson and J.-M. Mestdagh, *J. Phys. Chem. A*, 2007, **111**, 1771–1779.
202 B. Negru, G. M. P. Just, D. Park and D. M. Neumark, *Phys. Chem. Chem. Phys.*, 2011, **13**, 8180–8185.
203 B. C. Hoffman and D. R. Yarkony, *J. Chem. Phys.*, 2002, **116**, 8300–8306.
204 D. R. Yarkony, *J. Chem. Phys.*, 2005, **122**, 084316.
205 C. J. Xie, C. Malbon, D. R. Yarkony and H. Guo, *J. Chem. Phys.*, 2017, **146**, 224306.
206 C. P. Rodrigo, C. C. Zhou and H. Reisler, *J. Phys. Chem. A*, 2013, **117**, 12049–12059.
207 C. P. Rodrigo, S. Sutradhar and H. Reisler, *J. Phys. Chem. A*, 2014, **118**, 11916–11925.
208 C. L. Malbon and D. R. Yarkony, *J. Chem. Phys.*, 2017, **146**, 134302.
209 K. Samanta and D. R. Yarkony, *Chem. Phys.*, 2010, **378**, 110–117.
210 B. Karpichev, L. W. Edwards, J. Wei and H. Reisler, *J. Phys. Chem. A*, 2008, **112**, 412–418.
211 D. L. Osborn, D. J. Leahy and D. M. Neumark, *J. Phys. Chem. A*, 1997, **101**, 6583–6592.
212 A. E. Faulhaber, D. E. Szpunar, K. E. Kautzman and D. M. Neumark, *J. Phys. Chem. A*, 2005, **109**, 10239–10248.
213 B. L. J. Poad, A. W. Ray and R. E. Continetti, *J. Phys. Chem. A*, 2013, **117**, 12035–12041.
214 R. T. Bise, H. Choi, H. B. Pedersen, D. H. Mordaunt and D. M. Neumark, *J. Chem. Phys.*, 1999, **110**, 805–816.
215 S. H. S. Wilson, M. N. R. Ashfold and R. N. Dixon, *J. Chem. Phys.*, 1994, **101**, 7538–7547.
216 X. F. Zheng, Y. Song, J. Z. Wu and J. S. Zhang, *Chem. Phys. Lett.*, 2008, **467**, 46–51.
217 S.-K. Shih, S. D. Peyerimhoff and R. J. Buenker, *J. Mol. Spectrosc.*, 1979, **74**, 124–135.
218 D. Duflot, J.-M. Robbe and J.-P. Flament, *J. Chem. Phys.*, 1994, **100**, 1236–1246.
219 Q. Cui and K. Morokuma, *J. Chem. Phys.*, 1998, **108**, 626–636.
220 W. Y. Chiang and Y. C. Hsu, *J. Chem. Phys.*, 2000, **112**, 7394–7399.
221 A. M. Mebel, M. Hayashi, W. M. Jackson, J. Wrobel., M. Green, D. D. Xu and S. H. Lin, *J. Chem. Phys.*, 2001, **114**, 9821–9831.
222 A. Fahr, P. Hassanzadeh, B. Laszlo and R. E. Huie, *Chem. Phys.*, 1997, **215**, 59–66.
223 H.-J. Deyerl, I. Fischer and P. Chen, *J. Chem. Phys.*, 1999, **111**, 3441–3448.
224 S. J. Goncher, D. T. Moore, N. E. Sveum and D. M. Neumark, *J. Chem. Phys.*, 2008, **128**, 114303.
225 X. F. Zheng, Y. Song and J. S. Zhang, *J. Phys. Chem. A*, 2009, **113**, 4604–4612.
226 T. L. Nguyen, A. M. Mebel, S. H. Lin and R. I. Kaiser, *J. Phys. Chem. A*, 2001, **105**, 11549–11559.
227 B. M. Broderick, N. Suas-David, N. Dias and A. G. Suits, *Phys. Chem. Chem. Phys.*, 2018, **20**, 5517–5529.
228 D. L. Osborn, K. M. Vogelhuber, S. W. Wren, E. M. Miller, Y.-J. Lu, A. S. Case, L. Sheps, R. J. McMahon, J. F. Stanton, L. B. Harding, B. Ruscic and W. C. Lineberger, *J. Am. Chem. Soc.*, 2014, **136**, 10361–10372.
229 R. A. Seburg, E. V. Patterson and R. J. McMahon, *J. Am. Chem. Soc.*, 2009, **131**, 9442–9455.
230 J. Giegerich, J. Petersen, R. Mitrić and I. Fischer, *Phys. Chem. Chem. Phys.*, 2014, **16**, 6294–6302.
231 M. S. Schuurman, J. Giegerich, K. Pachner, D. Lang, B. Kiendl, R. J. MacDonell, A. Krueger and I. Fischer, *Chem. – Eur. J.*, 2015, **21**, 14486–14495.
232 B. Noller, M. Margraf, C. Schröter, T. Schultz and I. Fischer, *Phys. Chem. Chem. Phys.*, 2009, **11**, 5353–5357.
233 C. Groß, B. Noller and I. Fischer, *Phys. Chem. Chem. Phys.*, 2008, **10**, 5196–5201.
234 M. Ahmed, D. S. Peterka and A. G. Suits, *J. Chem. Phys.*, 1999, **110**, 4248–4253.
235 K. S. Xu and J. S. Zhang, *J. Chem. Phys.*, 1999, **111**, 3783–3786.
236 M. Shahu, C. H. Yang, C. D. Pibel, A. McIlroy, C. A. Taatjes and J. B. Halpern, *J. Chem. Phys.*, 2002, **116**, 8343–8352.
237 A. Fahr, P. Hassanzadeh and D. B. Atkinson, *Chem. Phys.*, 1998, **236**, 43–51.
238 A. M. Mann, X. Chen, V. A. Lozovsky and C. B. Moore, *J. Chem. Phys.*, 2003, **118**, 4452–4455.
239 P. Zhang, S. Irle, K. Morokuma and G. S. Tschumper, *J. Chem. Phys.*, 2003, **119**, 6524–6538.
240 L. Koziol, S. V. Levchenko and A. I. Krylov, *J. Phys. Chem. A*, 2006, **110**, 2746–2758.
241 M. Lucas, Y. Song, J. S. Zhang, C. Brazier, P. L. Houston and J. M. Bowman, *J. Phys. Chem. A*, 2016, **120**, 5248–5256.
242 M. L. Morton, J. L. Miller, L. J. Butler and F. Qi, *J. Phys. Chem. A*, 2002, **106**, 10831–10842.
243 Y. Song, M. Lucas, M. Alcaraz and J. S. Zhang, *J. Phys. Chem. A*, 2015, **119**, 12318–12328.
244 D. Stranges, M. Stemmler, X. M. Yang, J. D. Chesko, A. G. Suits and Y. T. Lee, *J. Chem. Phys.*, 1998, **109**, 5372–5382.
245 D. Stranges, P. O'Keeffe, G. Scotti, R. Di Santo and P. L. Houston, *J. Chem. Phys.*, 2008, **128**, 151101.
246 C. Chen, B. Braams, D. Y. Lee, J. M. Bowman, P. L. Houston and D. Stranges, *J. Phys. Chem. A*, 2011, **115**, 6797–6804.
247 H.-J. Deyerl, I. Fischer and P. Chen, *J. Chem. Phys.*, 1999, **110**, 1450–1462.
248 A. Röder, K. Issler, L. Poisson, A. Humeniuk, M. Wohlgemuth, M. Comte, F. Lepetit, I. Fischer, R. Mitric and J. Petersen, *J. Chem. Phys.*, 2017, **147**, 013902.
249 M. Shapero, I. A. Ramphal and D. M. Neumark, *J. Phys. Chem. A*, 2018, **122**, 4265–4272.
250 S. A. Ndenqué, R. Dawes and H. Guo, *J. Chem. Phys.*, 2016, **144**, 244301.
251 J. C. Loison, S. H. Kable, P. L. Houston and I. Burak, *J. Chem. Phys.*, 1991, **94**, 1796–1802.

252 D. W. Neyer, S. H. Kable, J. C. Loison, P. L. Houston, I. Burak and E. M. Goldfield, *J. Chem. Phys.*, 1992, **97**, 9036–9045.
253 S. H. Kable, J. C. Loison, D. W. Neyer, P. L. Houston, I. Burak and R. N. Dixon, *J. Phys. Chem.*, 1991, **95**, 8013–8018.
254 J. Riedel, S. Dziarzhytski, A. Kuczmann, F. Renth and F. Temps, *Chem. Phys. Lett.*, 2005, **414**, 473–478.
255 S. Y. Han, X. F. Zheng, S. Ndengue, Y. Song, R. Dawes, D. Q. Xie, J. S. Zhang and H. Guo, *Sci. Adv.*, 2019, **5**, eaau0582.
256 D. W. Neyer, X. Luo, I. Burak and P. L. Houston, *J. Chem. Phys.*, 1995, **102**, 1645–1657.
257 B. Rajakumar, J. E. Flad, T. Gierczak, A. R. Ravishankara and J. B. Burkholder, *J. Phys. Chem. A*, 2007, **111**, 8950–8958.
258 W. T. Mao, Q. Li, F. Kong and M. B. Huang, *Chem. Phys. Lett.*, 1998, **283**, 114–118.
259 S. K. Shin, S. K. Kim, H. L. Kim and C. R. Park, *J. Photochem. Photobiol., A*, 2001, **143**, 11–16.
260 D. L. Osborn, H. Choi, D. H. Mordaunt, R. T. Bise, D. M. Neumark and C. M. Rohlfing, *J. Chem. Phys.*, 1997, **106**, 3049–3066.
261 J. L. Miller, L. R. McCunn, M. J. Krisch, L. J. Butler and J. Shu, *J. Chem. Phys.*, 2004, **121**, 1830–1838.
262 C.-S. Lam, J. D. Adams and L. J. Butler, *J. Phys. Chem. A*, 2016, **120**, 2521–2536.
263 S. Matsika and D. R. Yarkony, *J. Chem. Phys.*, 2002, **117**, 7198–7206.
264 B. Nichols, E. N. Sullivan, M. Ryazanov and D. M. Neumark, *J. Phys. Chem. A*, 2017, **121**, 579–586.
265 E. J. Bernard, B. R. Strazisar and H. F. Davis, *Chem. Phys. Lett.*, 1999, **313**, 461–466.
266 A. Teslja, P. J. Dagdigian, M. Banck and W. Eisfeld, *J. Phys. Chem. A*, 2006, **110**, 7826–7834.
267 J. G. Radziszewski, *Chem. Phys. Lett.*, 1999, **301**, 565–570.
268 Y. Song, M. Lucas, M. Alcaraz, J. S. Zhang and C. Brazier, *J. Chem. Phys.*, 2012, **136**, 044308.
269 N. C. Cole-Filipiak, M. Shapero, B. Negru and D. M. Neumark, *J. Chem. Phys.*, 2014, **141**, 104307.
270 A. M. Mebel and A. Landera, *J. Chem. Phys.*, 2012, **136**, 234305.
271 Y. Song, X. F. Zheng, M. Lucas and J. S. Zhang, *Phys. Chem. Chem. Phys.*, 2011, **13**, 8296–8305.
272 M. Shapero, N. C. Cole-Filipiak, C. Haibach-Morris and D. M. Neumark, *J. Phys. Chem. A*, 2015, **119**, 12349–12356.
273 K. Pachner, M. Steglich, P. Hemberger and I. Fischer, *J. Chem. Phys.*, 2017, **147**, 084303.
274 M. Lucas, J. Minor and J. S. Zhang, *J. Phys. Chem. A*, 2013, **117**, 12138–12145.
275 M. Lucas, J. Minor, J. S. Zhang and C. Brazier, *Chin. J. Chem. Phys.*, 2014, **27**, 621–627.
276 E. Hébrard, M. Dobrijevic, Y. Bénilan and F. Raulin, *J. Photochem. Photobiol., C*, 2006, **7**, 211–230.
277 C. Møller and M. S. Plesset, *Phys. Rev.*, 1934, **46**, 618–622.
278 T. H. Dunning, Jr., *J. Chem. Phys.*, 1989, **90**, 1007–1023.
279 K. Andersson, P. A. Malmqvist, B. O. Roos, A. J. Sadlej and K. Wolinski, *J. Phys. Chem.*, 1990, **94**, 5483–5488.
280 B. O. Roos, P. Linse, P. E. M. Siegbahn and M. R. A. Blomberg, *Chem. Phys.*, 1982, **66**, 197–207.
281 M. J. Frisch, G. W. Trucks, H. B. Schlegel, G. E. Scuseria, M. A. Robb, J. R. Cheeseman, G. Scalmani, V. Barone, B. Mennucci, G. A. Petersson, H. Nakatsuji, M. Caricato, X. Li, H. P. Hratchian, A. F. Izmaylov, J. Bloino, G. Zheng, J. L. Sonnenberg, M. Hada, M. Ehara, K. Toyota, R. Fukuda, J. Hasegawa, M. Ishida, T. Nakajima, Y. Honda, O. Kitao, H. Nakai, T. Vreven, J. A. Montgomery Jr., J. E. Peralta, F. Ogliaro, M. Bearpark, J. J. Heyd, E. Brothers, K. N. Kudin, V. N. Staroverov, R. Kobayashi, J. Normand, K. Raghavachari, A. Rendell, J. C. Burant, S. S. Iyengar, J. Tomasi, M. Cossi, N. Rega, N. J. Millam, M. Klene, J. E. Knox, J. B. Cross, V. Bakken, C. Adamo, J. Jaramillo, R. Gomperts, R. E. Stratmann, O. Yazyev, A. J. Austin, R. Cammi, C. Pomelli, J. W. Ochterski, R. L. Martin, K. Morokuma, V. G. Zakrzewski, G. A. Voth, P. Salvador, J. J. Dannenberg, S. Dapprich, A. D. Daniels, Ö. Farkas, J. B. Foresman, J. V. Ortiz, J. Cioslowski and D. J. Fox, *Gaussian 09, Revis. B.01*, Gaussian, Inc., Wallingford, CT, 2009.